

PERFORMANCE STUDY ON COOLING OF
CONCENTRATOR PHOTOVOLTAICS USING
COMPUTATIONAL FLUID DYNAMICS SIMULATION

LEE SZE SHIN

MASTER OF ENGINEERING SCIENCE

FACULTY OF ENGINEERING AND SCIENCE
UNIVERSITI TUNKU ABDUL RAHMAN
NOVEMBER 2014

**PERFORMANCE STUDY ON COOLING OF CONCENTRATOR
PHOTOVOLTAICS USING COMPUTATIONAL FLUID DYNAMICS
SIMULATION**

By

LEE SZE SHIN

A dissertation submitted to the Department of Mechanical and Material
Engineering,
Faculty of Engineering and Science,
Universiti Tunku Abdul Rahman,
in partial fulfillment of the requirements for the degree of
Master of Engineering Science
November 2014

ABSTRACT

PERFORMANCE STUDY ON COOLING OF CONCENTRATOR PHOTOVOLTAICS USING COMPUTATIONAL FLUID DYNAMICS SIMULATION

Lee Sze Shin

Operating temperature of densely packed concentrator photovoltaic (CPV) system is vital. High concentration of solar irradiance focused onto the solar cells affect the solar-to-electrical conversion efficiency. Moreover, excessive thermal energy generated during the operation may reduce the life time or even damage the solar cells. Besides, non-uniform distribution of temperature across the solar cells connected in series leads to “current matching” problem, where the cell operated at the highest temperature will limit the conversion efficiency of the whole string. In this study, three-dimensional computational fluid dynamics (CFD) simulations were employed to investigate the effect of different inlet and outlet arrangements, fin designs and flow parameters on the cooling performance of cooling block in achieving lower as well as more uniform CPV temperature. The simulated result was validated with measured result, and a good agreement between both results was observed. From the simulations, it was found that different inlet/outlet arrangements could lead to significant changes in maximum CPV temperature and temperature uniformity. Also, the higher inlet flow rate and higher inlet/outlet area ratio led to the higher convective heat transfer between the coolant and cooling block. As a result, the CPVs would have a lower maximum operating temperature

and better temperature uniformity. Fin split has enhanced the performance of cooling block with center jet impingement design as it allows a more uniform flow distribution. Increment in fin width and reduction in spacing also improved the cooling performance as these increased the total convective heat transfer area to enhance the heat transfer from cooling block to coolant. However, it can be found that fin height and tip clearance had little effect on the cooling performance. The findings in this study may help in designing an effective cooling block for a CPV system and hence improve the solar-to-electrical conversion efficiency and prevent the system from permanent physical damage.

ACKNOWLEDGEMENT

I would like to express my deep and sincere gratitude to my supervisors, Dr. Lai Soon Onn and Prof. Chong Kok Keong. Throughout my project, they have provided encouragement, advice, guidance, support, and lots of good ideas. These have had a great influence on my entire project.

I wish to thank the faculty and staffs in Universiti Tunku Abdul Rahman, for providing assistance to my project. Special thank to the solar research team in Universiti Tunku Abdul Rahman for many helpful discussion and assistance during the course of my studies.

Last but not least, I wish to thank my grandmother, my parent, my brothers, my aunts, and Mei Sam, who were beside me all the time and gave me the needed support to complete my work.

APPROVAL SHEET

This dissertation entitled “**PERFORMANCE STUDY ON COOLING OF CONCENTRATOR PHOTOVOLTAICS USING COMPUTATIONAL FLUID DYNAMICS SIMULATION**” was prepared by LEE SZE SHIN and submitted as partial fulfillment of the requirements for the degree of Master of Engineering Science at Universiti Tunku Abdul Rahman.

Approved by:

(Dr. LAI SOON ONN)
Date:.....
Supervisor
Department of Chemical Engineering
Faculty of Engineering and Science
Universiti Tunku Abdul Rahman

(Prof. Dr. CHONG KOK KEONG)
Date:.....
Co-supervisor
Department of Electrical and Electronic Engineering
Faculty of Engineering and Science
Universiti Tunku Abdul Rahman

FACULTY OF ENGINEERING AND SCIENCE

UNIVERSITI TUNKU ABDUL RAHMAN

Date: 17 November 2014

SUBMISSION OF DISSERTATION

It is hereby certified that LEE SZE SHIN (ID No: 10UEM07357) has completed this dissertation entitled “PERFORMANCE STUDY ON COOLING SYSTEM OF CONCENTRATOR PHOTOVOLTAICS USING COMPUTATIONAL FLUID DYNAMICS SIMULATION” under the supervision of Dr. Lai Soon Onn (Supervisor) from the Department of Chemical Engineering, Faculty of Engineering and Science, and Prof. Dr. Chong Kok Keong (Co-Supervisor) from the Department of Electrical and Electronic Engineering, Faculty of Engineering Science

I understand that University will upload softcopy of my dissertation in pdf format into UTAR Institutional Repository, which may be made accessible to UTAR community and public.

Yours truly,

(LEE SZE SHIN)

DECLARATION

I hereby declare that the dissertation is based on my original work except for quotations and citations which have been duly acknowledged. I also declare that it has not been previously or concurrently submitted for any other degree at UTAR or other institutions.

Name LEE SZE SHIN

Date 17 November 2014

TABLE OF CONTENTS

	Page
ABSTRACT	ii
ACKNOWLEDGEMENT	iv
APPROVAL SHEET	v
SUBMISSION SHEET	vi
DECLARATION	vii
TABLE OF CONTENTS	viii
LIST OF TABLES	x
LIST OF FIGURES	xi
LIST OF ABBREVIATIONS	xiv
CHAPTER	
1.0 INTRODUCTION	1
1.1 Research Background	1
1.2 Research Aim and Objectives	3
1.3 Thesis Overview	3
2.0 LITERATURE REVIEW	5
2.1 Introduction to Solar Power	5
2.2 Cooling of Photovoltaic Cells	7
2.2.1 Single Cell Concentrator	7
2.2.2 Linear Concentrator	8
2.2.3 Dense Array Concentrator	9
2.3 Effect of Cell Temperature on Cell Conversion Efficiency	10
2.4 Non-imaging Planar Concentrator (NIPC)	11
2.5 Heat Transfer	13
2.5.1 Conduction	13
2.5.2 Convection	14
2.5.3 Radiation	15
2.6 Computational Fluid Dynamics	16
2.6.1 Solution Procedures of CFD	16
2.6.2 Applications of CFD in Solar Power System	17
3.0 METHODOLOGY	21
3.1 Experimental Method	21
3.2 Numerical Method	27
4.0 RESULTS AND DISCUSSIONS	37
4.1 CFD Validation	37
4.2 Effect of Inlet/Outlet Arrangement (Case Study 1)	38
4.3 Effect of Inlet Flow Rate (Case Study 2)	50
4.4 Effect of Fin Split (Case Study 3)	52
4.5 Effect of Fin Width (Case Study 4)	61

4.6	Effect of Fin Spacing (Case Study 5)	67
4.7	Effect of Inlet/Outlet Area Ratio (Case Study 6)	69
4.8	Effect of Fin Height (Case Study 7)	71
4.9	Effect of Tip Clearance (Case Study 8)	74
5.0	CONCLUSIONS AND FUTURE WORKS	78
5.1	Conclusions	78
5.2	Contributions	79
5.3	Future Works	81
	REFERENCES	82
	APPENDIX	91

LIST OF TABLES

Table		Page
3.1	Basic geometry parameters (in mm) of heat sink	25
3.2	Specifications of experimental setup	26
3.3	Summary of case studies	30
3.4	Geometrical parameters of inlets and outlets for cooling blocks	32
4.1	Comparison of simulated and measured temperatures of CPV and water outlet	38
4.2	Summary of effects of different parameter on cooling performance	77

LIST OF FIGURES

Figures	Page
2.1 Single cell concentrator (Royne et al., 2005)	8
2.2 Linear concentrator (Royne et al., 2005)	9
2.3 Dense array concentrator (Royne et al., 2005)	10
2.4 Comparison of different models for cell conversion efficiency at various temperatures summarized by Royne et al. (2005)	11
2.5 Conceptual layout design of NIPC (a) isometric view (b) cross-sectional view (Chong et al., 2009)	12
2.6 CFD modeling by Xing et al. (2014)	18
2.7 (a) Heat pipe cooling system and (b) CFD model by Anderson et al. (2008)	18
3.1 Prototype of non-imaging planar concentrator (Chong and Tan, 2012)	21
3.2 Symmetrical model of CPV receiver	22
3.3 CPV assembled on cooling block (Siaw et al., 2014)	23
3.4 Side view of CPV and bonding layers	23
3.5 Symmetrical geometry of heat sink: (a) isometric view (b) top view	24
3.6 Schematic diagram of coolant (water) flow direction	25
3.7 Inlet/outlet configurations for (a) Type-1 (b) Type-2 (c) Type-3 (d) Type-4 and (e) Type-5 cooling blocks	33
3.8 Geometries of heat sink with different fin splits (a) No-fin split (b) 1-fin split (c) 2-fin split (d) 3-fin split	35
3.9 Tip clearance	36

4.1	Infrared image of temperature distribution on the CPV receiver	37
4.2	Effect of inlet/outlet arrangement and coolant flow rate on maximum CPV temperature	39
4.3	Middle-plane velocity vector fields and average velocity at different channel for (a) Type-1 (b) Type-2 (c) Type-3 (d) Type-4 and (e) Type-5 at a coolant flow rate of $4 \times 10^{-4} \text{ m}^3/\text{s}$	42
4.4	Temperature contours for (a) Type-1 (b) Type-2 (c) Type-3 (d) Type-4 and (e) Type-5	46
4.5	Effect of inlet/outlet arrangement on CPV temperature uniformity	50
4.6	Effect of inlet flow rate on CPV temperature uniformity for Type-1 cooling block	52
4.7	Effect of fin split on maximum CPV temperature for (a) Type-1 (b) Type-2 and (c) Type-3	54
4.8	Velocity vector fields for (a) Type-1 (b) Type-2 and (c) Type-3 1-split design at a coolant flow rate of $4 \times 10^{-4} \text{ m}^3/\text{s}$	56
4.9	Velocity vector fields for Type-2 (a) 2-split and (b) 3-split cooling blocks at a coolant flow rate of $4 \times 10^{-4} \text{ m}^3/\text{s}$	58
4.10	Effect of fin split on CPV temperature uniformity for (a) Type-1 (b) Type-2 and (c) Type-3 cooling blocks	60
4.11	Effect of fin width on maximum CPV temperature for (a) Type-1 (b) Type-2 and (c) Type-3	63
4.12	Effect of fin width on CPV temperature uniformity for (a) Type-1 (b) Type-2 and (c) Type-3 cooling blocks	65
4.13	Effect of fin spacing on maximum CPV temperature	68
4.14	Effect of fin spacing on CPV temperature uniformity	69
4.15	Effect of inlet/outlet ratio on maximum CPV temperature	70

4.16	Effect of inlet/outlet ratio on CPV temperature uniformity	71
4.17	Effect of fin height on maximum CPV temperature	72
4.18	Effects of fin height on CPV temperature uniformity	73
4.19	Effect of tip clearance on maximum CPV temperature	74
4.20	Effect of tip clearance on CPV temperature uniformity	76

LIST OF ABBREVIATIONS

a	Distance between fin and heat sink wall (mm)
A	Area (m ²)
A_i	Total inlet area (mm ²)
A_o	Total outlet area (mm ²)
A_r	Total area of mirrors which reflect the solar flux to the target (m ²)
b	Distance between fin and heat sink wall (mm)
c	Thickness of heat sink wall (mm)
C_1	Turbulent constant
C_2	Turbulent constant
D	Distance between inlets and/or outlets (mm)
DNI	Direct normal irradiance (W/m ²)
G	Channel width (mm)
h	Convective heat transfer coefficient (W/m ² .K)
H_f	Height of fins (mm)
H_h	Height of heat sink (mm)
H_t	Height of top cover (mm)
k	Thermal conductivity (W/m.K)
K	Turbulent kinetic energy (m ² /s ²)
L_f	Length of fins (mm)
L_h	Length of heat sink (mm)
m	Solar cell efficiency parameter
n	Solar cell efficiency parameter
N_o	Number of outlets
P	Pressure (Pa)
P_{in}	Solar power input (W)
q	Heat energy (W)
r_i	Inlet radius (mm)

r_o	Outlet radius (mm)
T	Temperature (K)
T_∞	Fluid temperature (K)
u_i	Velocity components (m/s)
u_j	Velocity components (m/s)
W_f	Width of fins (mm)
W_h	Width of heat sink (mm)
W_i	Location of inlet (mm)
W_o	Location of outlet (mm)
W_t	Width of top cover (mm)
x_i	Coordinates (m)
x_j	Coordinates (m)

Greek symbols

η	Efficiency
ε	Turbulent energy dissipation rate (m^2/s^2)
ε_{rad}	Material emissivity
ρ	Density (kg/m^3)
μ_l	Laminar dynamic viscosity ($\text{N}\cdot\text{s}/\text{m}^2$)
μ_t	Turbulent dynamic viscosity ($\text{N}\cdot\text{s}/\text{m}^2$)
σ	Stefan–Boltzmann constant ($5.67 \times 10^{-8} \text{ W}/\text{m}^2\cdot\text{K}^4$)
σ_k	Turbulent constant
σ_ε	Turbulent constant
σ_l	Laminar Prandtl number
σ_t	Turbulent Prandtl number

Subscripts

amb	Ambient
c	Solar cell
$cond$	Conduction
$conv$	Convection
i	i -direction

<i>j</i>	<i>j</i> -direction
<i>rad</i>	Radiation
<i>s</i>	Surface
<i>l</i>	Laminar
<i>t</i>	Turbulent

CHAPTER 1

INTRODUCTION

1.1 Research Background

The entire collective surface of conventional flat photovoltaic (PV) system is made of relatively costly solar cells. Hence, it increases the installation cost for the system. In order to reduce the cost, concentrator photovoltaic (CPV) system was introduced in 1970s where optical elements such as mirrors and lenses, which are less costly compared with solar cells, are used to focus a higher amount of solar irradiance onto a smaller area (Swanson, 2000). In this way, the total number of solar cells required and hence the installation cost for the system can be reduced. However, during the operation, large amount of excessive heat will be generated. This excessive and unwanted heat will reduce the efficiency of solar-to-electrical conversion. Besides, if the temperature is higher than the permitted limit, it may reduce the life time of solar cells or cause permanent degradation (Dalal and Moore, 1977; Mbewe et al., 1985; Sala, 1989; Royne et al., 2005; Skoplaki and Palyvos, 2009). Akbarzadeh and Wadowski (1996) studied the cooling of solar cells with concentrated solar radiation and reported that a 50 % reduction in solar cell performance was observed when the surface temperature of the cell increased from 46 to 84 °C. Teo et al. (2012) also found that solar cells could only achieve efficiency of 8-9 % without active cooling, but it could be

improved to 12-14 % with active cooling. Therefore, it can be concluded that the effectiveness of cooling system in a CPV is important to maximize the efficiency of solar-to-electrical conversion as well as to increase the life time of the solar cells.

On the other hand, for solar cells in dense-array layout, non-uniform distribution of temperature can also affect the overall conversion efficiency (Mathur et al., 1984; Luque et al., 1998; Antón et al., 2001; Baig et al., 2012; Ben Or and Appelbaum, 2013). Royne et al. (2005) reported that solar cells that were electrically connected in series had an advantage of lower Ohmic losses. However, the major problem of applying series connection is “current matching”, where the solar cell which gives the smallest output current will limit the overall current. As increment in solar cell temperature reduces its efficiency, the output current of the whole string will be limited by the cell that is operated at the highest temperature.

However, there are not many works related to the investigation on the effects of flow parameters and fin designs on the CPV cooling in the literature. Hence, in the current study, the performance of the CPV cooling system was investigated by studying the effects of various flow parameters and fin designs on the maximum operating temperature and temperature uniformity of solar cells for dense-array CPV. Computational fluid dynamics (CFD) was used as a tool for the simulation study. In order to validate the simulated result, on-site data collection was conducted using non-imaging planar concentrator (NIPC) prototype.

1.2 Research Aim and Objectives

The aim of this study was to design a novel and effective cooling system for a CPV.

The objectives of this study were:

1. To determine the influences of various flow parameters (inlet/outlet arrangement, inlet flow rate and inlet/outlet area ratio)
2. To determine the influences of various fin design parameters (fin split, fin width, fin spacing, fin height and tip clearance)

on the temperature uniformity and maximum operating temperature of dense-array CPV.

1.3 Thesis Overview

The outline of thesis is given as follows:

Chapter 1 presents a general introduction, objectives to be achieved as well as the layout of the thesis.

Chapter 2 covers a literature review which includes an introduction of solar power, cooling of photovoltaic cells in different concentrators, effect of cell temperature on its efficiency and introduction of NIPC. A basic theory for heat transfer, which includes conduction, convection and radiation, is also presented in this chapter. Lastly, brief introduction on the principles of CFD

and the solution procedures for CFD are included. Reviews on applications of CFD in solar system are presented as well.

Chapter 3 describes the experimental setup of NIPC used in this study, including the geometries of cooling block and cooling system, optical arrangement, CPV cells arrangement and solar irradiance during the experiment. Besides, a description on the CFD simulation setup, including the setting of parameters in the software, equations used for computation, models developed for CFD simulations, mesh generations as well as the case studies conducted, is also included.

In Chapter 4, on-site data collected is used to validate the CFD model developed. The CFD simulation is subsequently used to study the effect of each parameter on the maximum CPV operating temperature and temperature uniformity of CPV cells. The results are analyzed and compared in this chapter as well.

Chapter 5 highlights the conclusions and the contributions of this thesis as well as some improvements that can be made and recommended in the future study.

CHAPTER 2

LITERATURE REVIEW

2.1 Introduction to Solar Power

When the sunlight passes through the atmosphere, the solar constant is reduced from its initial solar irradiance of about 1,353 W/m² to about 1,000 W/m². This reduction in solar constant is due to Rayleigh scattering by molecules, aerosols and dusts in the atmosphere. Besides, some of the solar energy may be absorbed by the gases such as oxygen, ozone and water vapour as well as re-radiation of the solar back into the space. As a result, only about 1,000 W/m² of solar energy left when it reaches the ground if the weather is clear. However, it should be highlighted that this amount of energy can be varied according to different atmospheric conditions and movement of Earth with respect to the sun (Brogren, 2004).

Brogren (2004) grouped the utilization of solar energy, according to their energy output, to three categories, which are solar thermal collectors, photovoltaic system and photovoltaic-thermal system. These systems are also identified to be as an active solar energy system, where mechanical or electronics hardware is required. As an opposite, passive solar energy system does not require the aid of hardware.

In solar thermal collectors, solar energy is converted into thermal energy. Gas or liquid is allowed to flow around a circuit to absorb the solar energy as thermal for further use. The United States Energy Information Administration (EIA) has classified solar thermal collectors into three categories, which are low-, medium-, or high-temperature collectors according to their operating temperature. For the low-temperature collectors, generally a lower grade of heat is available for heating, especially used in heating water or space. Where else, the medium-temperature collectors, which usually use flat plates as the collector, are mainly used in domestic heating. Evacuated-tube collector is also grouped under this category as well. As for the high-temperature collectors, the sunlight is generally concentrated with the use of mirrors or lenses. High-temperature collectors are usually used in industries and electrical power production.

Photovoltaic (PV) system converts solar radiation into direct current (DC) electricity with the use of semiconductors. Photovoltaic effect takes place in the conversion, where photons of sunlight excite the electrons in the PV and allow them to act as charge carriers for electric current. PV cells can be electrically connected together to form photovoltaic modules in order to deliver more power. Royne et al. (2005) has grouped different PV systems according to their geometries. This will be discussed in the next section.

Photovoltaic/thermal hybrid (PV/T) solar system combines both photovoltaic and solar thermal systems into one. Therefore, it is capable of producing both electricity and heat from one integrated system. In the PV/T

system, the PVs are used to generate electricity, while the solar thermal collector acts as a thermal absorber which absorbs the remaining heat from the PV module as well as to removes the waste heat in order to ensure that the PV modules work at a suitable temperature (Chow, 2010).

2.2 Cooling of Photovoltaic Cells

Royne et al. (2005) grouped different concentrators according to their geometries as various concentrator geometries require considerably different cooling methods. The types of concentrator geometries are single cell, linear geometry and dense-array. In the following section, different concentrator systems and the respective cooling technique for each type will be discussed.

2.2.1 Single Cell Concentrator

In a single cell system, different types of lenses are commonly used for concentration. For this type of concentrator, the sunlight is focused onto each cell individually. Hence, in order to ensure that the CPV cell is fully illuminated under the high concentration sunlight, a focused sunlight area of equal or bigger than the area of CPV cell is necessary. As shown in Figure 2.1, a larger heat sinking area can be allocated for single cell system. Dashed lines in Figure 2.1 show the area available for heat sinking. Therefore passive cooling can be used (Royne et al., 2005).

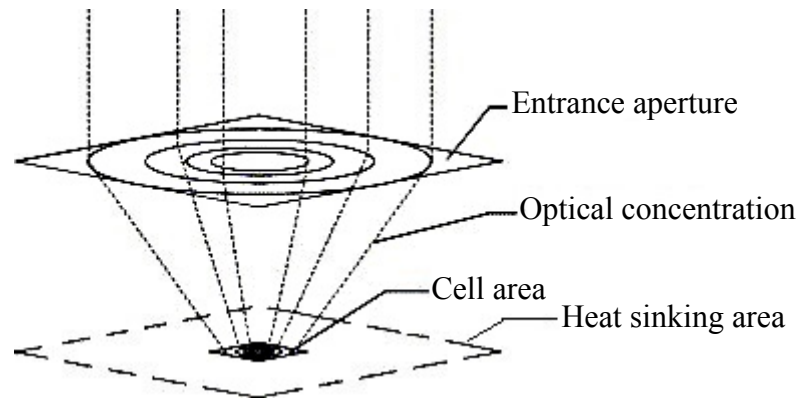


Figure 2.1: Single cell concentrator (Royne et al., 2005)

2.2.2 Linear Concentrator

In linear concentrator, parabolic troughs and Frensel lenses are used to focus the sunlight onto CPV cells. As shown in Figure 2.2, as CPV cells are arranged in a row, the available area for heat dissipation is less because the cells are in close contact with neighbouring cells. Dashed lines in Figure 2.2 demonstrate the area available for heat sinking. Both passive and active cooling can be used to remove heat generated by the linear concentrator (Royne et al., 2005).

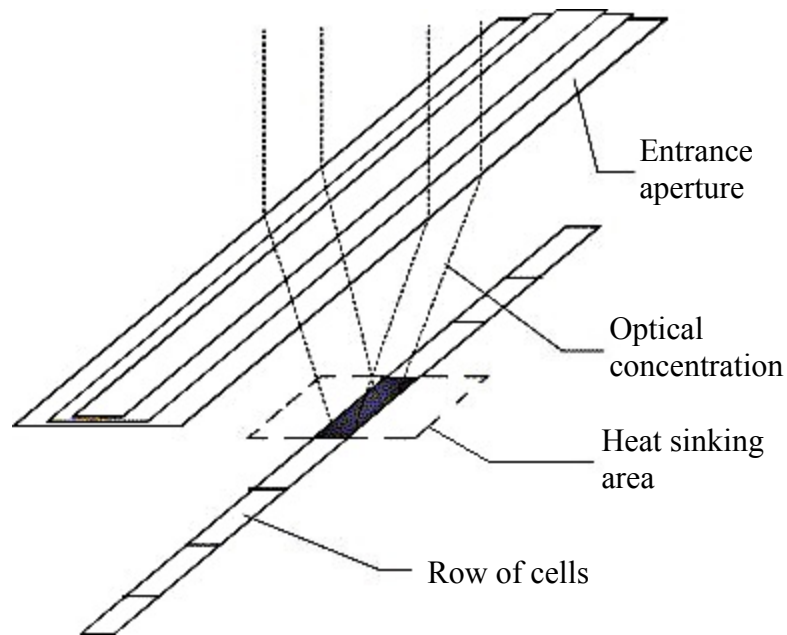


Figure 2.2: Linear concentrator (Royne et al., 2005)

2.2.3 Dense Array Concentrator

In a dense array concentrator such as heliostat, parabolic dish or non-imaging planar concentrator (NIPC), CPV cells are densely packed on the receiver, where each cell is surrounded by neighbouring cells on four sides. Cooling of such system is more difficult than the previous two types as heat can only be dissipated through the rear surface of the cells, except for cells located at the edges of the module, as illustrated in Figure 2.3. Besides, the area of illumination onto the dense array CPV module and level of sunlight concentration are also higher than the previous two geometries. It results in the highest amount of excessive energy. This implies that passive cooling is not suitable to be used for dense array configuration (Royne et al., 2005).

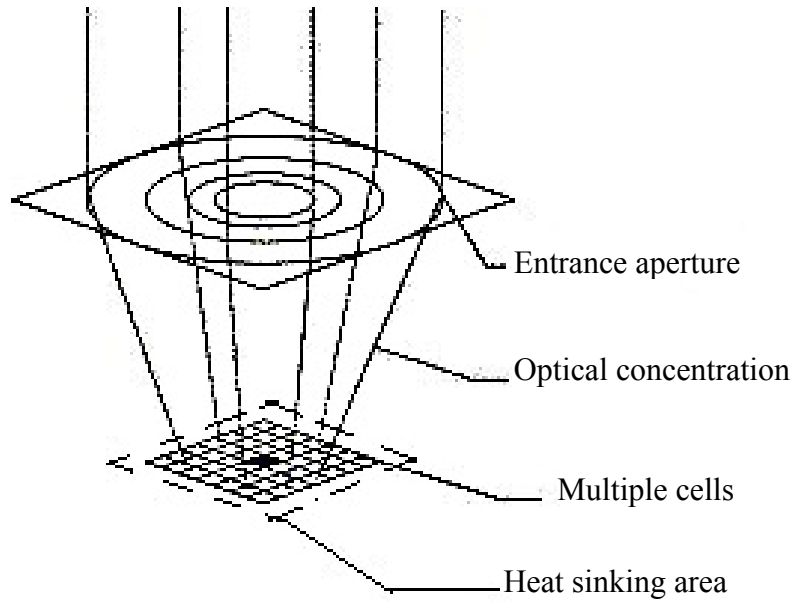


Figure 2.3: Dense array concentrator (Royne et al., 2005)

2.3 Effect of Cell Temperature on Cell Conversion Efficiency

Both cell temperature and solar illumination are important to the cell solar-to-electrical conversion efficiency. Royne et al. (2005) summarized various models found in literature (Figure 2.4). As shown in Figure 2.4, the cell conversion efficiency reduced linearly with increment in cell temperature. A simple model is thus developed, with the assumption of a linear decrement in the cell efficiency (Equation 2.1) with increase in the temperature and no dependency on concentration:

$$\eta = m(1 - nT_c) \quad (2.1)$$

where η is the solar-to-electrical conversion efficiency of the cell at a given temperature of T_c , m and n are constants which depend on the solar cell material.

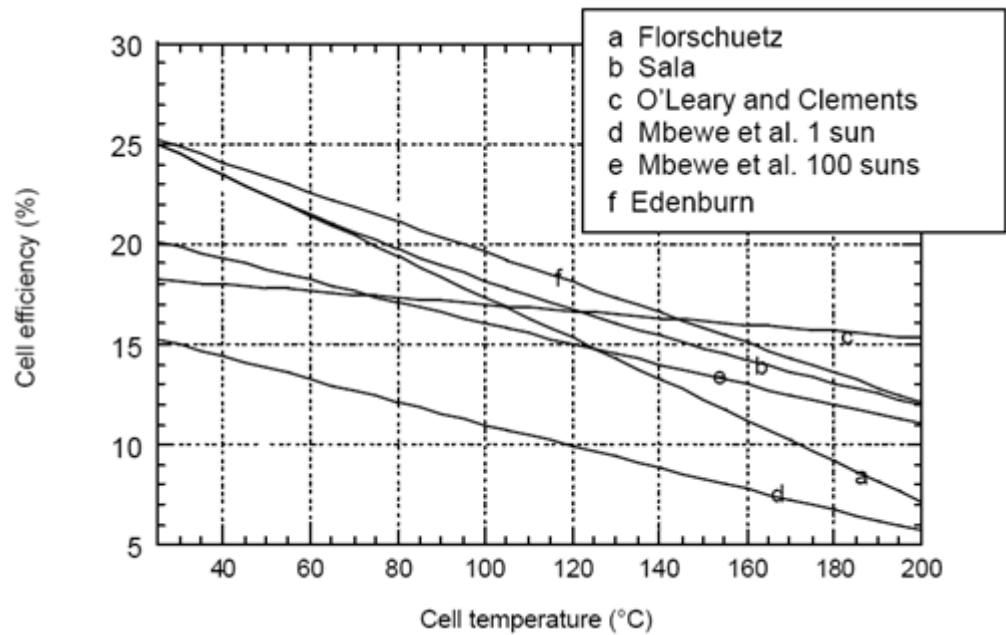


Figure 2.4: Comparison of different models for cell conversion efficiency at various cell temperatures summarized by Royne et al. (2005)

2.4 Non-imaging Planar Concentrator (NIPC)

NIPC has been introduced with the goal of achieving better solar irradiation uniformity and at the same time resulting in a reasonable high ratio of sunlight concentration on the target. In the NIPC, the concept of non-imaging optics is applied, where square flat mirrors will be used as optical aperture with the purpose of collecting and focusing the incident sunlight onto the target. Figure 2.5 demonstrates the conceptual layout design of the NIPC and how solar rays are directed onto the target by individual mirror in the system. In terms of concentrating incident sunlight, the idea is similar to that of non-imaging focusing heliostat. As shown in Figure 2.5(b), by superpositioning the flat mirror images into one, uniform intensity can be

achieved. Hence, in the NIPC, an array of flat mirrors is used to reflect the incident sunrays onto the target. Hence, the size as well as the shape of the reflected image are nearly same as those of the receiver (Chong et al., 2009).

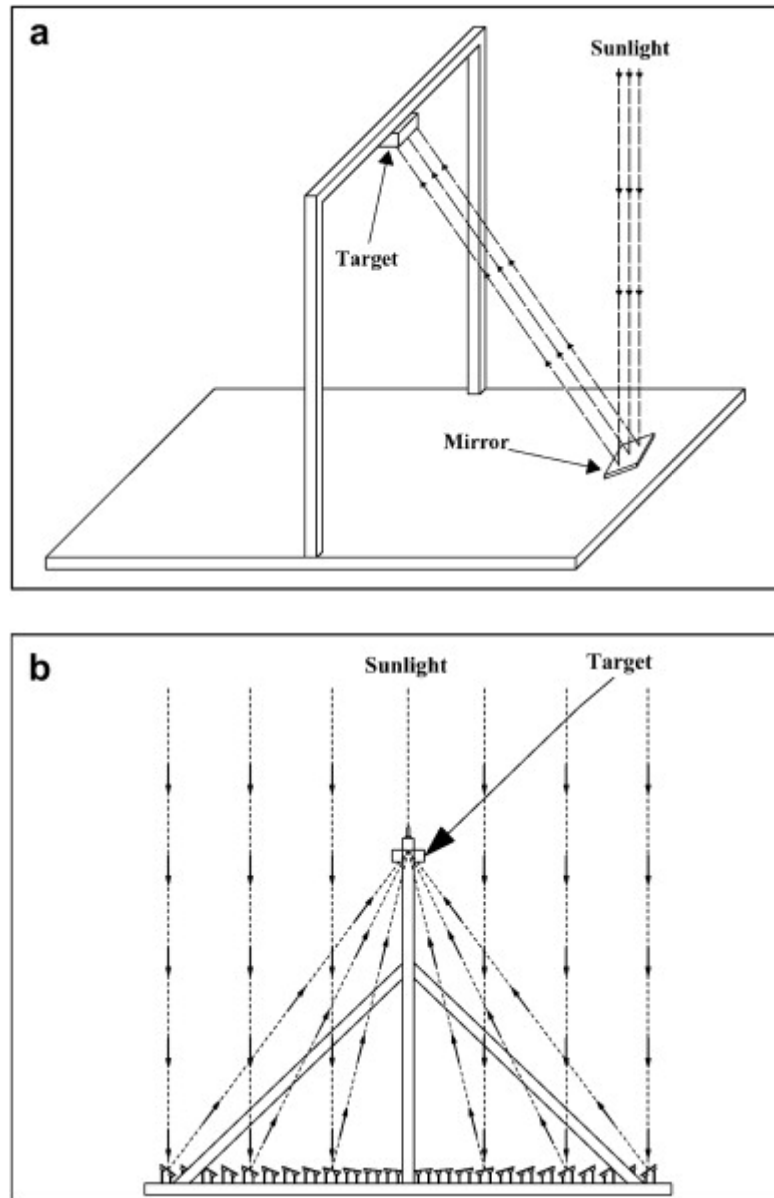


Figure 2.5: Conceptual layout design of NIPC (a) isometric view (b) cross-sectional view (Chong et al., 2009)

2.5 Heat Transfer

Heat transfer is the science that predicts the energy transfer that may take place between material bodies as a result of temperature difference. The science of heat transfer is also important in predicting the rate at which the exchange takes place under a specific condition (Holman, 2002). Heat transfer can be categorized into three types, which are conduction, convection and radiation.

2.5.1 Conduction

Heat conduction is the transfer of internal energy by microscopic diffusion and collisions of particles within a body due to a temperature gradient. Heat conduction can also be viewed as energy is transferred from more energetic particles to less energetic particles due to the interactions between particles. Rate equations can be used to quantify the processes of heat transfer, where the amount of energy transferred per unit time can be calculated. The rate equation for conduction is one-dimensional known as Fourier's Law (Equation 2.2):

$$q_{cond} = -kA \frac{dT}{dx} \quad (2.2)$$

where q_{cond} (W) is the conductive heat transfer, A is the area perpendicular to the direction of heat transfer (m^2), $\frac{dT}{dx}$ (K/m) represents the temperature gradient and k (W/m.K) is the thermal conductivity of the material (Bergman et al., 2011).

In this study, conduction was considered in the heat transfer among the CPV cells, bonding layers and cooling block.

2.5.2 Convection

Convective heat transfer comprises of two mechanisms, which are energy transfer as a result of random molecular motion (diffusion) and energy transfer as a result of bulk, or macroscopic, motion of the fluid. In convective heat transfer, the interaction between moving fluid and its bounded surface due to difference in temperature is especially important (Bergman et al., 2011).

Convective heat transfer can be classified according to the nature of the flow, into forced convection and free (or natural) convection. When the flow is caused by external means, such as by a fan, a pump, or atmospheric winds, forced convection occurs. In contrast, there are some cases where the flow is induced by buoyancy forces, a result of density difference caused by temperature variations in the fluid. This process is known as free convection (Bergman et al., 2011).

In order to calculate the heat transfer, the rate equation of convection, is expressed as

$$q_{conv} = hA(T_s - T_\infty) \quad (2.3)$$

It is known as Newton's law of cooling, where q_{conv} is the convective heat transfer (W), A is the area for heat transfer (m^2), h is the convective heat transfer coefficient ($W/m^2.K$) and T_s and T_∞ are the surface temperature (K)

and fluid temperature (K), respectively. The value of convective heat transfer coefficient depends on the conditions in the boundary layer, which are influenced by surface geometry, nature of the fluid motion, and an assortment of fluid thermodynamic and transport properties (Bergman et al., 2011). In this work, heat transfer between the cooling block and coolant was categorized as forced convection.

2.5.3 Radiation

Thermal radiation is a type of heat transfer where the energy emitted by nonzero temperature substance. The energy is transported by electromagnetic waves. The emission is related to energy released due to the oscillations or transitions of the electrons that constitute matter. These oscillations are, in turn, sustained by the internal energy, and therefore the temperature of the matter. Hence the emission of thermal radiation is associated with thermally excited conditions within the matter. Different from conduction or convection, where the transfer of energy requires the presence of a material medium, radiation does not. Hence, radiation transfer occurs most effectively in a vacuum. The rate equation of radiation heat transfer is stated as

$$q_{rad} = \varepsilon_{rad} A \sigma (T_s^4 - T_{amb}^4) \quad (2.4)$$

where q_{rad} is the radiation heat transfer (W), A is the area for heat transfer (m^2), σ is the Stefan–Boltzmann constant ($5.67 \times 10^{-8} \text{ W/m}^2 \cdot \text{K}^4$), T_s is the surface temperature of radiating body (K) and T_{amb} is the temperature of the environment (K). ε_{rad} is the material emissivity, which is a measure that

shows how effectively a surface emits energy relative to a black body. It ranges from 0 to 1 and depends strongly on the surface material and finish (Bergman et al., 2011).

2.6 Computational Fluid Dynamics

Computational Fluid Dynamics (CFD) is a simulation of fluid flow phenomena in an engineering system using modeling (mathematical physical problem formulation) and numerical methods (discretization methods, solvers, numerical parameters, and grid generations, etc.).

2.6.1 Solution Procedures of CFD

To solve and obtain result from the CFD, the following solution procedures are normally performed (Çengel and Cimbala, 2009).

1. The geometry or computation domain of the problem is defined.
2. The volume occupied by the fluid is divided into discrete element, called as cells (or mesh). The meshes generated may be uniform or non-uniform. The CFD solution is highly dependent on the quality of the meshes. Therefore, the mesh quality should be checked by conducting grid independence test.
3. Numerical parameters and solution algorithm such as continuity equation, momentum equation, energy equation, turbulence models, pressure-velocity coupling are selected.

4. Boundary conditions are specified on the edge or face of the domain.
5. Types and properties such as temperature, density, viscosity of the domain are specified.
6. The equations are solved iteratively with initial conditions, until a converged solution is obtained.
7. Finally, once the solution has converged, the result is plotted and analyzed.

2.6.2 Applications of CFD in Solar Power System

CFD simulations have been widely used in analyzing the heat removal performance of various designs for lowering the temperature of solar cells.

Studies have been conducted to investigate different geometrical parameters on cooling of solar cells using CFD simulations. Xing et al. (2014) studied the effects of tilt angle and air gap size on photovoltaic module performance using CFD (Figure 2.6) and found that the efficiency and tilt angle relationship showed different behaviour at different wind velocities. For instance, the module efficiency was maximum when the tilt angle reached 90 °.

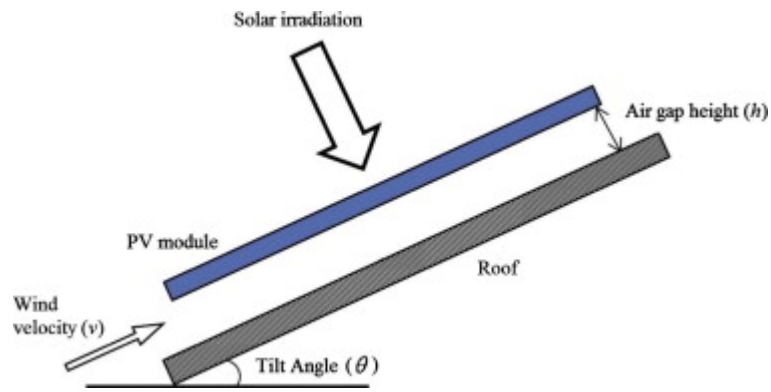
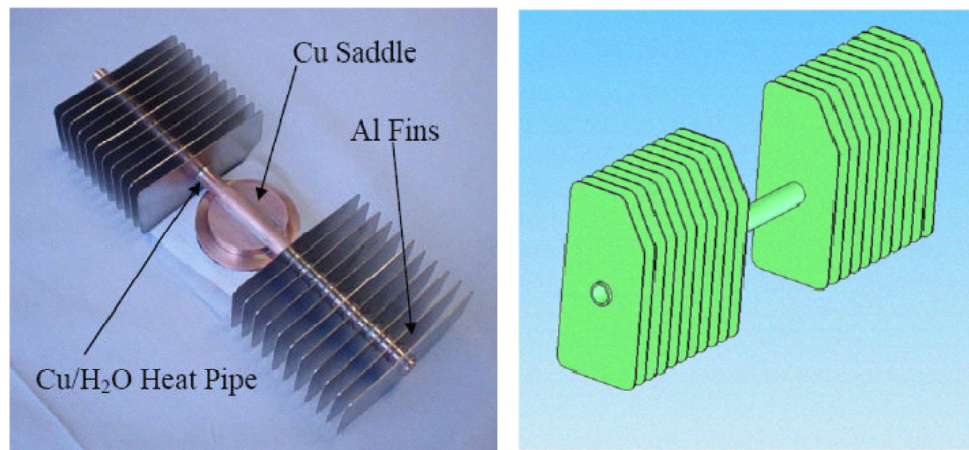


Figure 2.6: CFD modeling by Xing et al. (2014)

Besides, Anderson et al. (2008) investigated the performance of heat pipe on cooling of CPV systems using CFD. Figure 2.7 presents the heat pipe cooling system and CFD model used. It was found that the optimum fin pitch was 7.94 mm.



(a)

(b)

Figure 2.7: (a) Heat pipe cooling system and (b) CFD model by Anderson et al. (2008)

CFD simulation has also been used to study the effect of environment such as ambient temperature on cooling of solar cells. Wang et al. (2013) investigated the dissipation of heat generated from a high-concentration

photovoltaic (HCPV) module with the aid of numerical computations. The journal concluded that the relation of maximum cell temperature with ambient temperature and direct normal irradiance was a linear function. The simulation results also indicated that the maximum temperature of the HCPV module could be reduced when the wind speed increased. A three dimensional CFD model was developed by Siddiqui et al. (2012) to simulate the performance of PV modules at different ambient temperature, with and without cooling. It was found that when the ambient temperature increased from 0 to 50 °C, electrical power decreased from 98 to 92.5 W for PV module with cooling. However, at the same temperature range, electrical power decreased from 95.7 to 47.2 W for PV module without cooling.

Also, CFD simulations were used to investigate the performance of thermal solar hybrid system and liquid immersion cooling. Teo et al. (2012) investigated the temperature profile for a hybrid PV/T thermal solar system through experimental and simulation models with and without active cooling. It was found that the trend between the cell's temperature and conversion efficiency was linear and about 5% improvement could be achieved with active cooling. Zhu et al. (2010) used simulation model to investigate the performance of liquid-immersion cooling for densely packed solar cells and conclude that the solar cells average temperature increased when the flow velocity decreased.

Validation studies have also been carried out to compare the experimental results with three dimensional CFD models. Natarajan et al.

(2011) validated the simulation results for a concentrating photovoltaic system with experimental results by comparing the solar cells and lens temperature. The results showed a good agreement (deviation of 3.8 %). Besides, Gray et al. (2007) modelled a passive cooling system for photovoltaic cells and compared the chamber air temperature with experimental results. A small deviation of 3 % was also observed.

Most of the studies have shown good agreement between experimental and simulated results. Hence, it can be concluded that CFD is a promising method to investigate the thermal performance of cooling system for PV system.

CHAPTER 3

METHODOLOGY

3.1 Experimental Method

Figure 3.1 shows the prototype of NIPC designed and built at Universiti Tunku Abdul Rahman (UTAR), Kuala Lumpur, Malaysia. The prototype comprised of 404 flat mirrors and a total reflective area of 4.04 m² (Siaw et al., 2014). The incident sunlight was focused onto a receiver placed at a focal distance of 1.7 m.

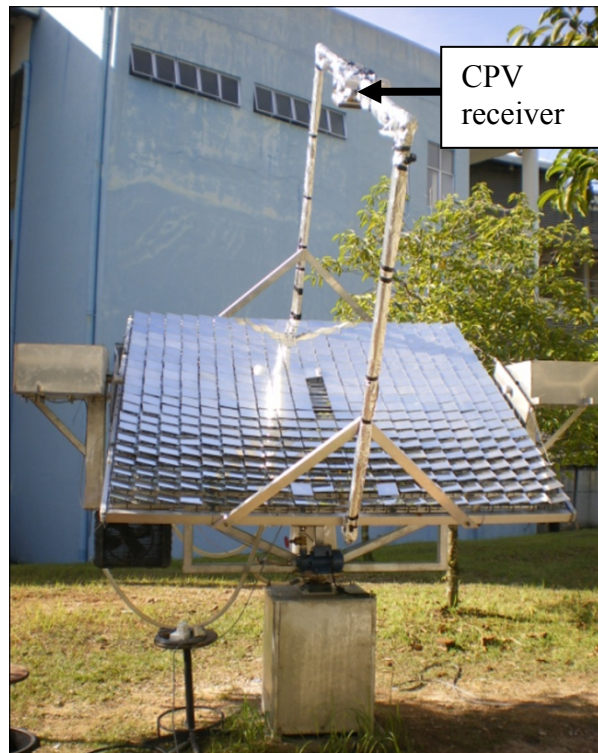


Figure 3.1: Prototype of non-imaging planar concentrator (Chong and Tan, 2012)

Figure 3.2 illustrates the symmetrical model of the CPV receiver. The CPV receiver consisted of four major parts, i.e., copper heat sink, aluminium cover, CPV panel with thermal bonding layers and water inlet/outlet manifold. The CPV panel consisted of 44 pieces of CPV cells each with a size of 10 mm (L) \times 10 mm (W) (Figure 3.3). The CPV cells were assembled on the cooling block together with the bonding layers consisting of the following materials: solder, copper layer in direct bond copper (DBC) substrate, alumina layer in DBC substrate, copper layer in DBC substrate and artic silver thermal adhesive. Figure 3.4 is an enlarged cross sectional view of the CPV cell and bonding layers to show the order and the thickness of different layers.

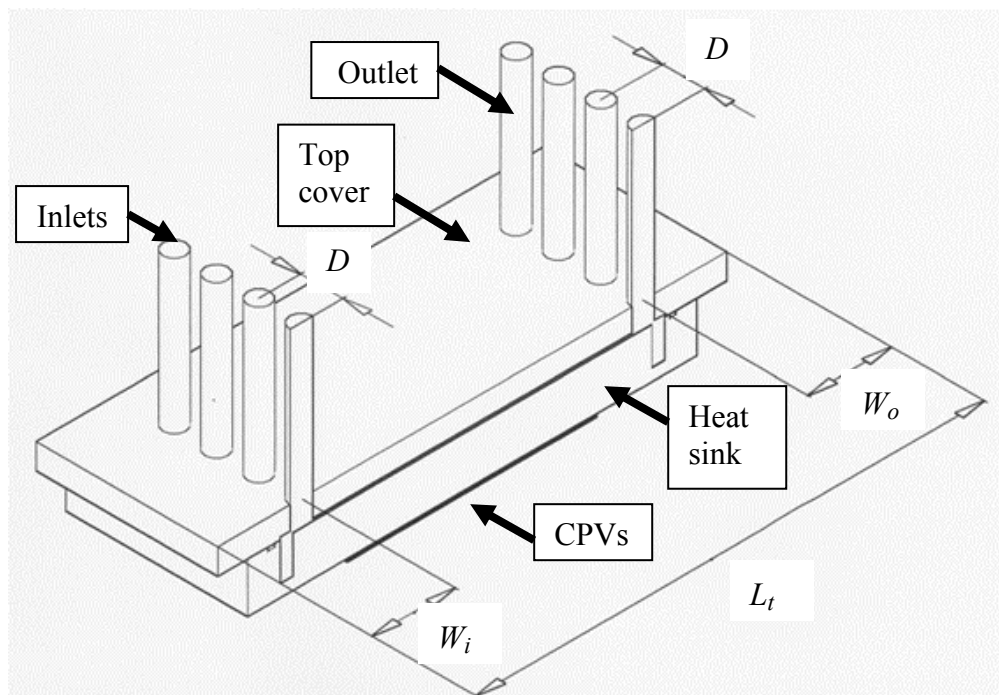


Figure 3.2: Symmetrical model of CPV receiver

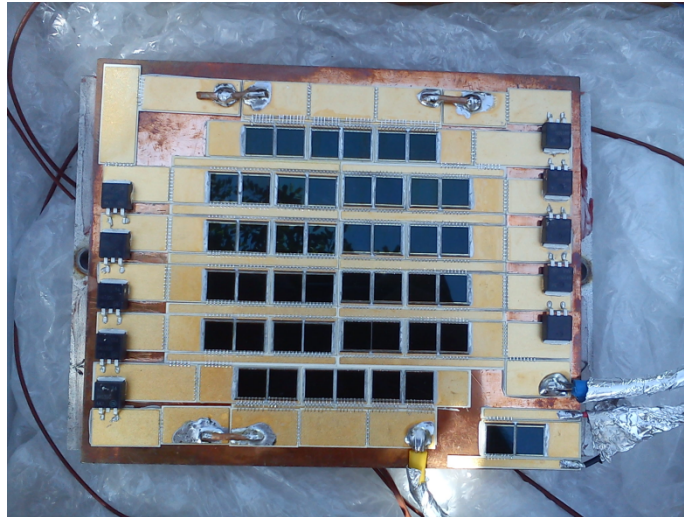


Figure 3.3: CPV assembled on cooling block (Siaw et al., 2014)

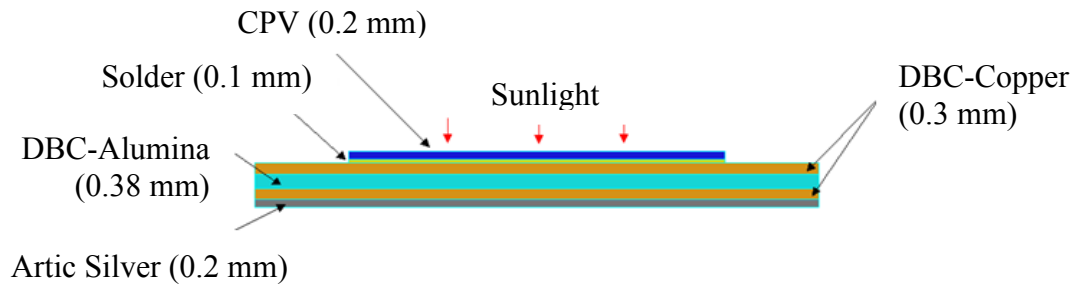
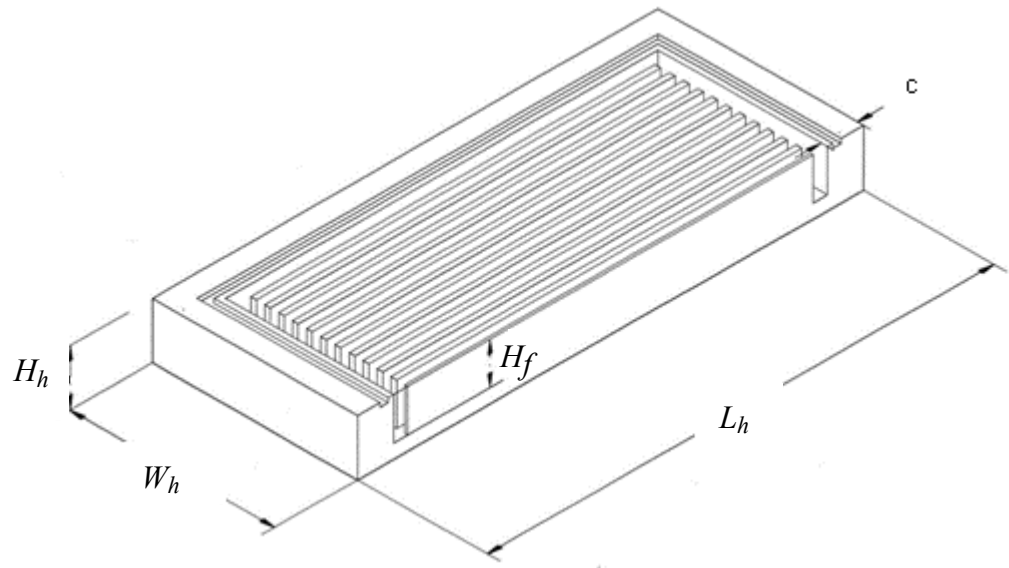
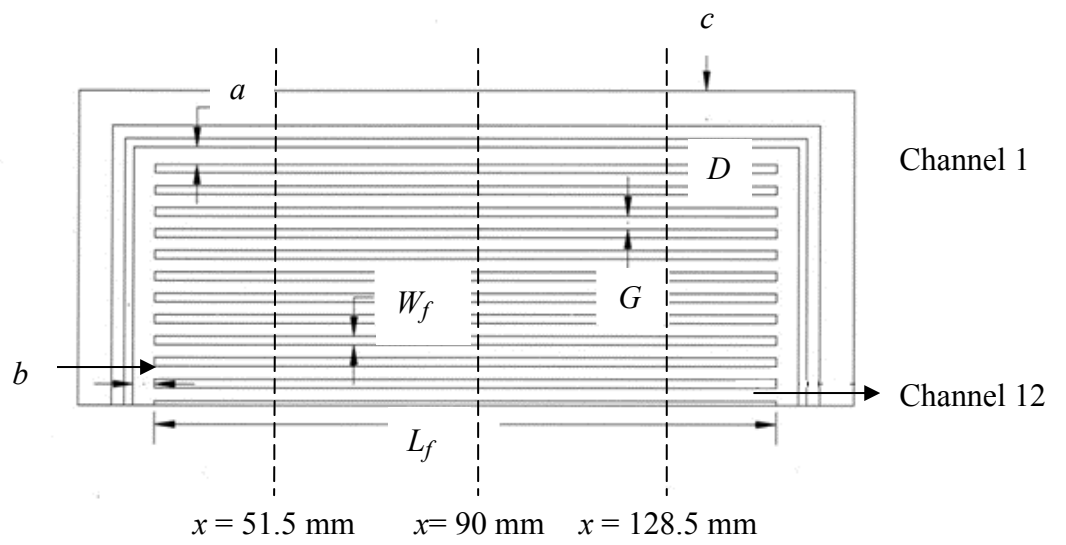


Figure 3.4: Side view of CPV and bonding layers

The heat sink was comprised of 23 rectangular fins with a width of 2 mm and a height of 15 mm. Figure 3.5 depicts the symmetrical model of heat sink. All the fins had a length of 144 mm with 3 mm spacing between two fins. Geometrical parameters of heat sink are provided in Table 3.1. The dimensions of aluminium cover were 204 mm (L) \times 73 mm (W) \times 10 mm (H).



(a)



(b)

Figure 3.5: Symmetrical geometry of heat sink: (a) isometric view (b) top view

Table 3.1: Basic geometry parameters (in mm) of heat sink

W_h	73	L_f	144
L_h	180	H_f	15
H_h	20	G	3
a	4	W_t	73
b	5	L_t	204
c	13	H_t	10
W_f	2		

Figure 3.6 shows the schematic diagram of coolant flow direction in the experimental setup. During the operation, water was used as the coolant fluid and was continuously pumped from a reservoir tank to the cooling block which was attached to the receiver holder frame by a submersible pump with a rated power of 100 W. Water entered the cooling block through seven inlets at a constant flow rate of $3.8 \times 10^{-4} \text{ m}^3/\text{s}$. Excessive heat generated from the concentrated sunlight was absorbed by the water which subsequently left the cooling block from seven outlets located at another side and was finally released to the environment. Table 3.2 summarizes the specifications of the experimental setup.

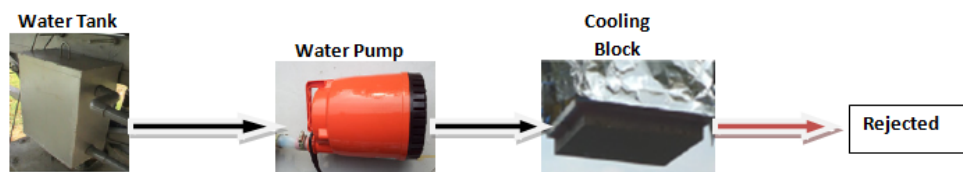


Figure 3.6: Schematic diagram of coolant (water) flow direction

Table 3.2: Specifications of experimental setup

Concentrator Photovoltaic System

Latitude	3.2° N
Longitude	107.7° E
Focal distance	1.7 m
Total number of mirrors	404
Total reflective area, A_r	4.04 m ²
Cooling block	
Rated power of pump	100 W
Water flow rate	3.8×10^{-4} m ³ /s
Inlet temperature	303 K

At the site, with the use of pyr heliometer (The Eppley Laboratory Model NIP), direct normal irradiance (DNI) was measured and used to calculate the solar power input, P_{in} (W) of the system as expressed in Equation 3.1:

$$P_{in} = \eta \times DNI \times A_r \quad (3.1)$$

where $\eta = 0.8$ is the direct conversion efficiency including the reflection loss of mirror and the absorptivity of cooling block from solar to thermal energy and A_r is the total reflective area of the NIPC prototype (Chong and Tan, 2012).

In order to measure the temperature at the outlet, thermocouple was used. Besides, the temperature distribution on the CPV receiver was measured

using infrared thermal imaging camera (FLIR Model i5). Experimental results collected from the site were used to validate the accuracy of the CFD model.

3.2 Numerical Method

Three dimensional CFD commercial software, ANSYS Fluent 14.0 (ANSYS, 2011), was used to study both the flow field and temperature field of the model. The following assumptions were made during the simulation:

1. the system was in steady state;
2. the flow was incompressible and turbulent;
3. the flow was symmetrical;
4. the solid and fluid properties such as density, thermal conductivity, specific heat capacity and viscosity were constant;
5. except the bottom surface of the CPV panel, the rest of the external walls were assumed to be perfectly insulated. Therefore, the heat loss to the environment through radiation and convection could be ignored.

A uniform heat flux with an area of 10 cm (L) \times 10 cm (W) was considered to illuminate on the bottom surface of the CPV panel. To represent the fluid flow, $k - \varepsilon$ turbulence model was adopted. The governing equations are expressed as follows:

Continuity equation:

$$\frac{\partial \rho \bar{u}_i}{\partial x_i} = 0 \quad (3.2)$$

Momentum equation:

$$\rho \bar{u}_j \frac{\partial \bar{u}_i}{\partial x_j} = -\frac{\partial \bar{p}}{\partial x_i} + \frac{\partial}{\partial x_j} \left[\mu_t \left(\frac{\partial \bar{u}_i}{\partial x_j} + \frac{\partial \bar{u}_j}{\partial x_i} \right) \right] \quad (3.3)$$

Energy equation:

$$\rho \bar{u}_j \frac{\partial \bar{T}}{\partial x_j} = \frac{\partial}{\partial x_j} \left[\left(\frac{\mu_l}{\sigma_l} + \frac{\mu_t}{\sigma_t} \right) \frac{\partial \bar{T}}{\partial x_j} \right] \quad (3.4)$$

Turbulent kinetic energy (k) equation:

$$\rho \bar{u}_j \frac{\partial k}{\partial x_j} = \frac{\partial}{\partial x_i} \left(\frac{\mu_t}{\sigma_k} \frac{\partial k}{\partial x_i} \right) + \mu_t \left(\frac{\partial \bar{u}_i}{\partial x_j} + \frac{\partial \bar{u}_j}{\partial x_i} \right) \frac{\partial \bar{u}_i}{\partial x_j} - \rho \varepsilon \quad (3.5)$$

Turbulent kinetic energy dissipation (ε) equation:

$$\rho \bar{u}_j \frac{\partial \varepsilon}{\partial x_j} = \frac{\partial}{\partial x_j} \left(\frac{\mu_t}{\sigma_\varepsilon} \frac{\partial \varepsilon}{\partial x_j} \right) + C_1 \mu_t \frac{\varepsilon}{k} \left(\frac{\partial \bar{u}_i}{\partial x_j} + \frac{\partial \bar{u}_j}{\partial x_i} \right) \frac{\partial \bar{u}_i}{\partial x_j} - C_2 \rho \frac{\varepsilon^2}{k} \quad (3.6)$$

In the simulation, inlet temperature was set to be 303 K. The thermal conductivities for copper heat sink, aluminium cover and water were 400, 202, and 0.6 W/m.K, respectively, while the thermal conductivities for CPV, solder material, copper layer in DBC substrate, alumina layer in DBC, copper layer in DBC substrate and artic silver thermal adhesive were 55, 29, 400, 24, 400 and 7.5 W/m.K, respectively (Luque et al., 2007). Identical to the experimental setup, water was used as coolant fluid in the numerical computations.

Tetrahedral meshes were used for cooling block, aluminium cover and water mesh generation, while hexagonal meshes were used for CPV layers. Grid independence analysis was carried out to ensure that the optimum mesh size was selected in the study. The pressure and velocity fields were decoupled using the semi-implicit method for a pressure-linked equation (SIMPLE). The convergence criterion was defined as 10^{-4} for the scaled residual for all the equations. In this study, only half section of cooling block was simulated in order to save computational time since the flow was symmetrical.

Table 3.3 summarized all the case studies conducted in this work. Case Study 1 investigated the effect of five inlet/outlet arrangements. In Case Studies 3 and 4, Types-1, 2 and 3 were adopted. Types-4 and 5 were not considered due to the poorer cooling performance compared to Types-1, 2 and 3 (refer to Section 4.2 Effect of inlet/outlet arrangement). Type-2 design with 1-fin split was adopted in Case Studies 5 to 8 as it had the greatest improvement in cooling performance compared to Types-1 and 3 (refer to Section 4.4 Effect of Fin Split). In Case Study 7, the fin heights of 10, 15 and 20 mm were used. This could be justified by the finding that the fin height had a slight influence on cooling performance compared to the findings in Case Studies 1 to 6 (refer to Section 4.8 Effect of Fin Height). In Case Study 8, increment in tip clearance also showed insignificant effects (refer to Section 4.9 Effect of Tip Clearance). Therefore, tip clearance of 1, 2 and 3 mm were considered.

Table 3.3: Summary of case studies

Case study	Inlet/outlet arrangement	Fin split	Fin width (mm)	Fin spacing (mm)	Inlet/outlet area ratio	Fin height (mm)	Tip clearance (mm)
1. Inlet/outlet arrangement	Types-1,2,3,4 and 5	No	2	3	1	15	1
2. Inlet flow rate	Type-1	No	2	3	1	15	1
3. Fin split	Types-1,2 and 3	No, 1-, 2- and 3- split	2	3	1	15	1
4. Fin width	Types-1,2 and 3	1-split	1, 2, 3	3	1	15	1
5. Fin spacing	Type-2	1-split	2	2, 3, 4	1	15	1
6. Inlet/outlet area ratio	Type-2	1-split	2	3	0.5, 1.0, 1.5	15	1
7. Fin height	Type-2	1-split	2	3	1	10, 15, 20	1
8. Tip clearance	Type-2	1-split	2	3	1	15	1, 2, 3

Case Study 1: Inlet/outlet arrangement

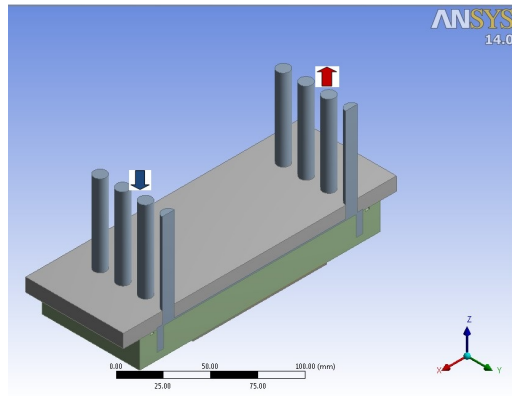
As shown in Figure 3.7, five types of cooling blocks were designed to analyze the effect of different inlet/outlet arrangements on cooling performance of CPV. Dimensions of the heat sink for these five cooling blocks were identical to the prototype as reported in Table 3.1, except for location and size of the inlets and outlets. Type-1 had the exact same location and size of inlets and outlets with the prototype. It was chosen in the comparison between the simulation and experimental results in this study. Type-2 had a single inlet with a radius of 11.9 mm which was located at the center of the cooling block, while four outlets with identical radius of 4.5 mm were located at one side of the cooling block. It should be noted that the total inlet area still remained the same with the total outlet area. Type-3 had a single inlet with a radius of 16.84 mm which was located at the center of the cooling block, while four outlets with a radius of 4.5 mm were located at both sides of the cooling block. The geometrical dimensions for Types-4 and 5 were the same with those for Types-2 and 3, with the only modification by swapping the inlet and outlet locations and hence reversing the flow direction as well. Table 3.4 summarizes the geometrical parameters of inlets and outlets for all the cooling blocks. Heat sink without fin split was used in this case study.

The five types of inlet/outlet arrangement were designed in order to investigate the difference between incoming flow from side (Type-1, 4 and 5) with impinging inlet at the center (Type-2 and 3). In addition, the influence of reversing the flow direction could be studied by comparing the results between Type-2 and 4 as well as between Type-3 and 5. Furthermore, Type-3 and 4

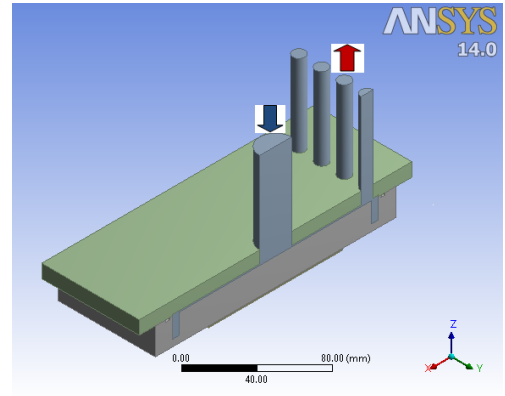
were also used in order to study the effect of different outlet locations. On the other hand, the radii for the inlets and outlets were calculated and selected in such a way that the total inlet area was identical to the total outlet area (i.e., inlet/outlet area ratio=1).

Table 3.4: Geometrical parameters of inlets and outlets for cooling blocks

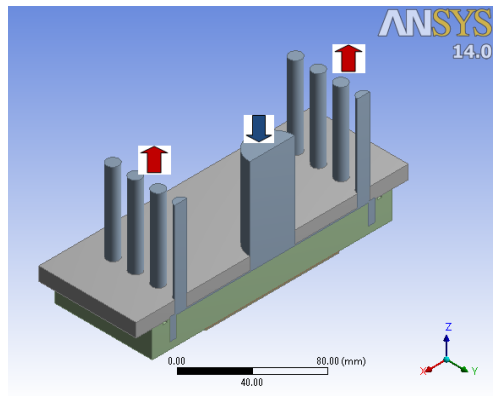
Type	1	2	3	4	5
Inlet radius, r_i (mm)	4.5	11.9	16.84	4.5	4.5
Location of inlet, W_i (mm)	8.5	120	120	8.5	8.5
Number of inlets, N_i	3.5	0.5	0.5	3.5	7
Total inlet area, A_i (mm ²)	222	222	445	222	445
Outlet radius, r_o (mm)	4.5	4.5	4.5	11.9	16.84
Location of outlet, W_o (mm)	8.5	8.5	8.5	120	120
Number of outlets, N_o	3.5	3.5	7	0.5	0.5
Total outlet area, A_o (mm ²)	222	222	445	222	445
Distance between inlets or outlets, D (mm)	17	17	17	17	17



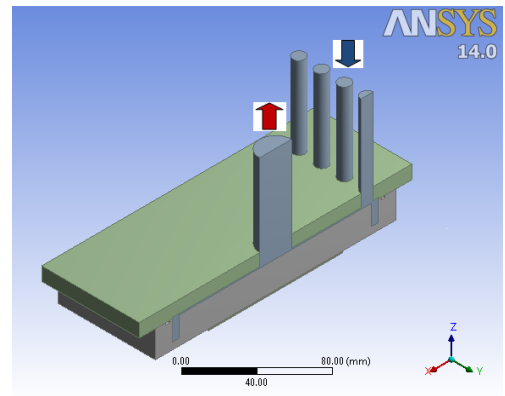
(a)



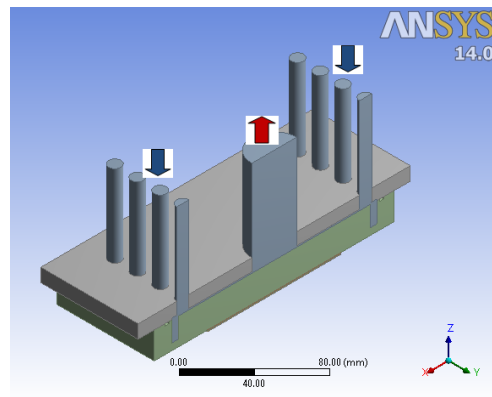
(b)



(c)



(d)



(e)

Figure 3.7: Inlet/outlet configurations for (a) Type-1 (b) Type-2 (c) Type-3 (d) Type-4 and (e) Type-5 cooling blocks

Case Study 2: Inlet flow rate

In Case Study 2, the effect of inlet flow rate on maximum temperature and temperature uniformity of CPV were investigated. Type-1 inlet/outlet configuration was used in the numerical computations, while the geometries of the heat sink are presented in Table 3.1.

Case Study 3: Fin split

Four different fin split designs (No-, 1-, 2- and 3-fin split) were used in this study. Basic geometries of heat sink were the same as Table 3.1, but additional fin splits of width 4 mm were introduced as shown in Figure 3.8. In this study, Types-1, 2 and 3 inlet/outlet configurations were used for computations.

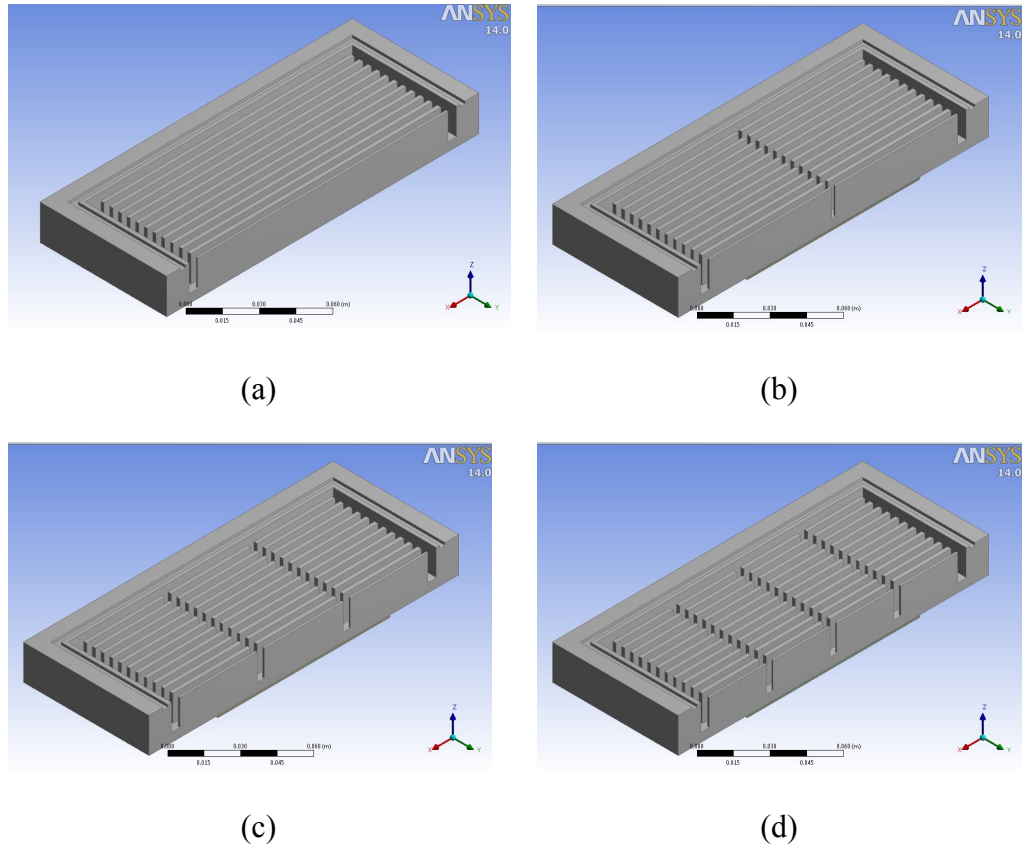


Figure 3.8: Geometries of heat sink with different fin splits (a) No-fin split (b) 1-fin split (c) 2-fin split (d) 3-fin split

Case Study 4: Fin width

Effect of fin width on maximum temperature and temperature uniformity of CPV were investigated in Case Study 4. Types-1, 2 and 3 inlet/outlet configurations with 1-fin split were used in this study, while other geometrical parameters of cooling block remained identical to the dimensions listed in Table 3.1.

Case Studies 5, 6, 7 and 8

Effects of fin spacing, inlet/outlet area ratio, fin height and tip clearance (the height between top cover and tip of fins (Figure 3.9)) on maximum temperature and temperature uniformity of CPV were investigated in Case Studies 5, 6, 7 and 8, respectively. Type-2 inlet/outlet configuration with 1-fin split was used. In order to study the effects, only the stated parameter was varied, while the rest of the geometrical parameters were fixed.

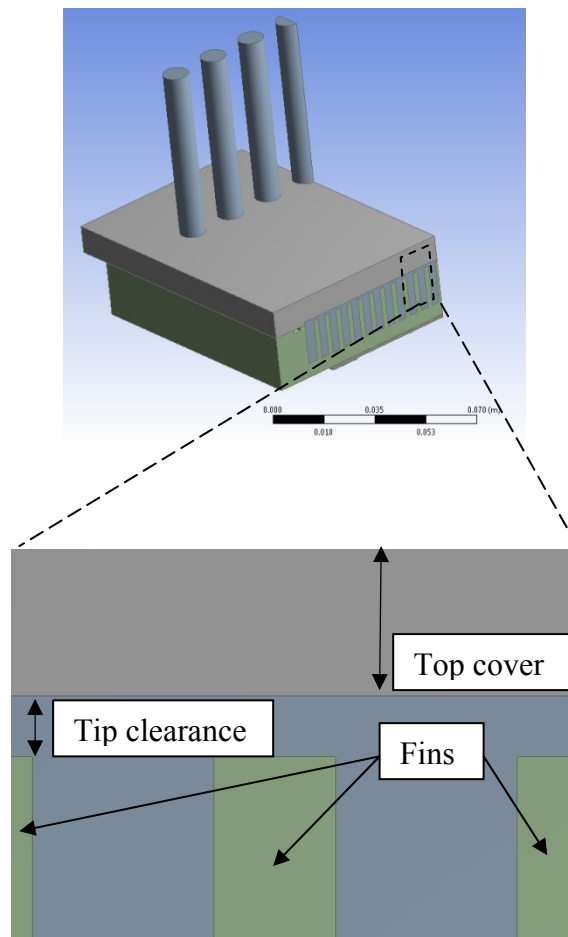


Figure 3.9: Tip clearance

CHAPTER 4

RESULTS AND DISCUSSIONS

4.1 CFD Validation

At the site, solar power input of $227,000 \text{ W/m}^2$ and water outlet temperature of 304.5 K were measured using pyrhelimeter and thermocouple, respectively on 9/10/2012. Besides, as illustrated in Figure 4.1, the temperature distribution on the CPV receiver was measured using infra-red thermal imaging camera on the same day. Subsequently, the mean temperature (325.6 K) of the targeted location (represented with a black circle in Figure 4.1) on the CPV was reported.

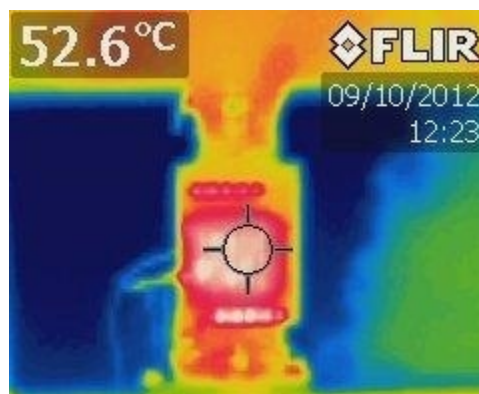


Figure 4.1: Infrared image of temperature distribution on the CPV receiver

Type-1 cooling block, with the identical geometry (Table 3.1) and inlet/outlet arrangement with the prototype, was used in the grid independence

analysis. Solar power input (227,000 W/m²) measured during the experiment was applied to the simulation model. Three total numbers of grids used were 238,249, 2,803,006 and 4,963,801. A CPV temperature deviation of 4 K was noticed for the number of grids of 238,249. By increasing the number of grids to 2,803,006, the temperature deviation reduced to 2.07 K. However, further refining the number of grids to 4,963,801 only reduced the deviation to 1.56 K. Hence, to save computing time, grid system of 2,803,006 was applied for this study. Table 4.1 shows the comparison of simulated and measured results for the grid system of 2,803,006 and a good agreement was observed. The deviations between simulated and measured temperatures of CPV and water outlet were 0.638 and 6.57×10^{-3} %, respectively.

Table 4.1: Comparison of simulated and measured temperatures of CPV and water outlet

Location	Temperature		
	Simulated (K)	Measured (K)	Deviation (%)
CPV	327.67	325.6	0.638
Water outlet	304.48	304.5	6.57×10^{-3}

4.2 Effect of Inlet/Outlet Arrangement (Case Study 1)

Figure 4.2 illustrates the effect of inlet/outlet arrangement on the maximum CPV temperature, where a significant effect was noticed. When the

flow rates were identical for all five types, a maximum temperature difference of up to 4 K was observed for different inlet/outlet arrangements. Type-1 cooling block was noticeably the design with the best cooling performance as the maximum operating temperature of CPV cells was the lowest among all the five designs. The cooling block with center jet impingement (Types-2 and 3) were in fact expected to perform better in the preliminary stage due to higher fluid flow velocity at zone of concentrated high temperature. This discrepancy was possibly due to the fact that the coolant flow direction was restricted by the long rectangular fins of heat sink, resulting in poorer cooling performance.

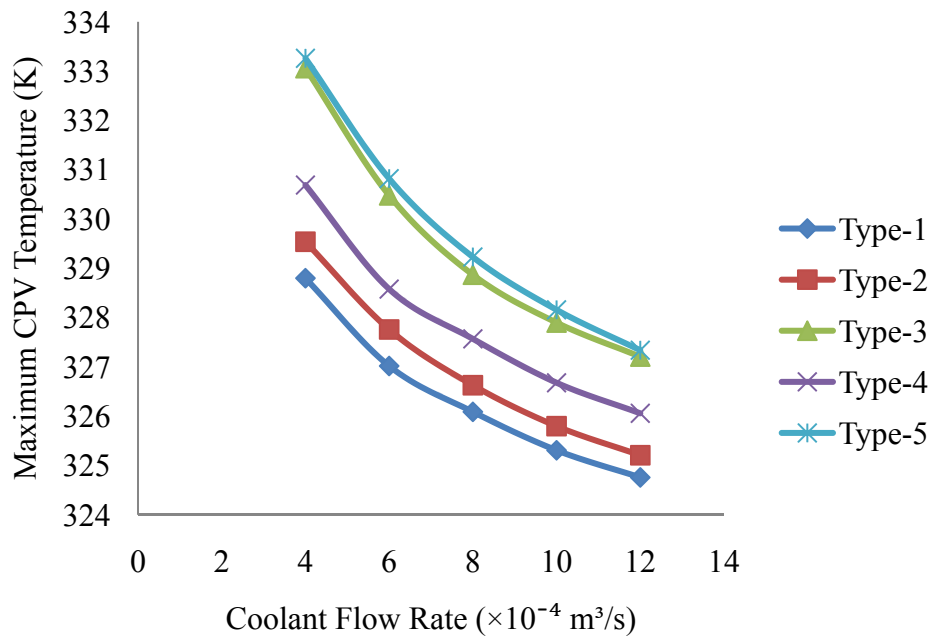


Figure 4.2: Effect of inlet/outlet arrangement and coolant flow rate on maximum CPV temperature

Figure 4.3 shows the middle-plane velocity vectors field (12.5 mm above heat sink base) and average velocity at each channel while Figure 4.4

illustrates the temperature contours of all five types of cooling block at a coolant flow rate of $4 \times 10^{-4} \text{ m}^3/\text{s}$. In Type-1 cooling block, it could be seen that the flow was able to distribute evenly between channels and maintain at a relatively high coolant flow velocity (Figure 4.3(a)). Variation between the channels of highest and lowest velocity was only 0.2 m/s.

The Nusselt number (Nu) is defined as

$$Nu = \frac{hD_h}{k} \quad (4.1)$$

where h is the convective heat transfer coefficient ($\text{W}/\text{m}^2\cdot\text{K}$), D_h is the hydraulic diameter (m) and k ($\text{W}/\text{m}\cdot\text{K}$) is the thermal conductivity of the fluid.

For forced convection, the Nusselt number can also be expressed as a function of Reynold number (Re) and Prandtl number (Pr)

$$Nu = f(Re, Pr) \quad (4.2)$$

$$Re = \frac{\rho v D_h}{\mu} \quad (4.3)$$

$$Pr = \frac{C_p \mu}{k} \quad (4.4)$$

where ρ is the density (kg/m^3), v is the velocity (m/s), μ is the viscosity ($\text{kg}/(\text{m}\cdot\text{s})$) and C_p is the specific heat capacity ($\text{J}/(\text{kg}\cdot\text{K})$) of the fluid.

Based on Equations 4.1, 4.2 and 4.3, it could be concluded that increased in the fluid velocity would resulted in a higher convective heat transfer coefficient. As a result, the convective heat transfer were higher according to Equation 2.3

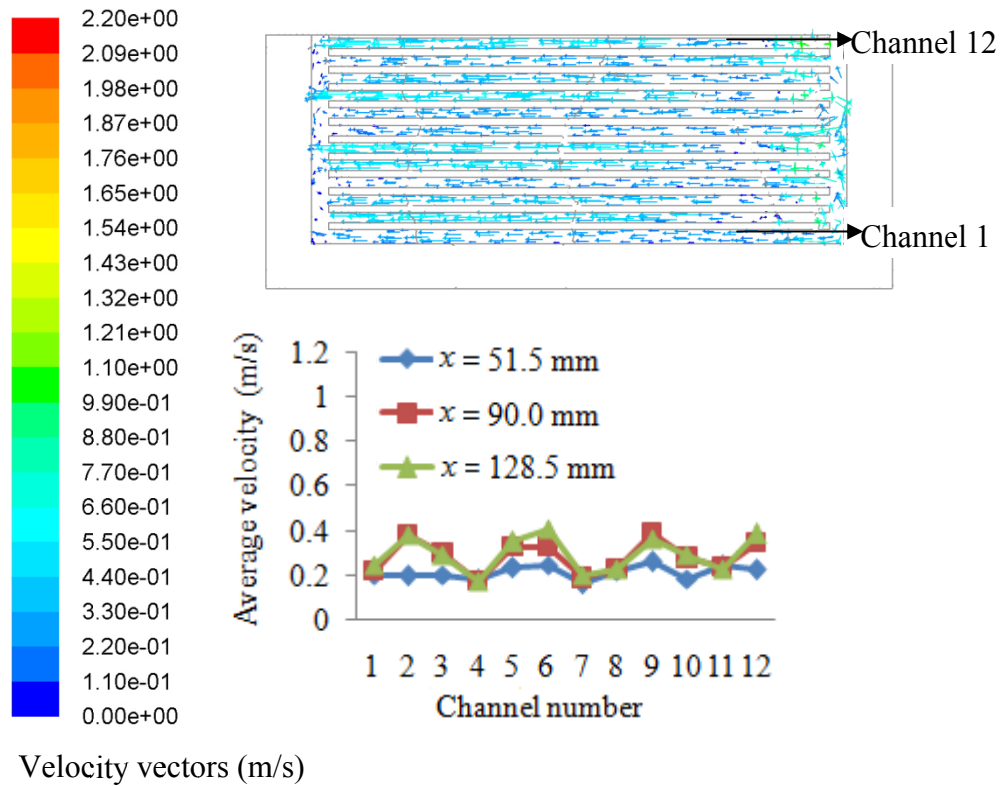
$$q_{conv} = hA(T_s - T_\infty) \quad (2.3)$$

Hence, the high coolant flow velocity in Type-1 encouraged the forced convection, and hence more effectively reduced the fin temperature and eventually resulted in a greater reduction in the CPV temperature.

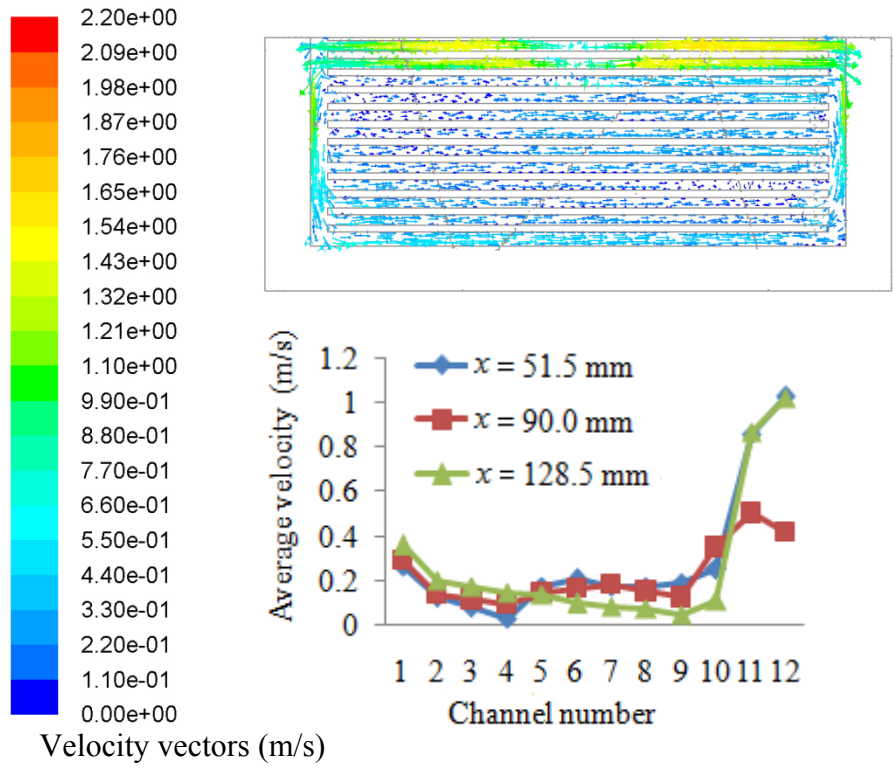
It should be highlighted that Types-2 and 3 cooling block had a jet impingement design. The coolant entering the cooling blocks from the center was unable to be effectively distributed to the surrounding channels (Channels 1 to 10) and resulted in a significant drop of flow velocity (Figures 4.3(b) and (c)). For example, the channel located below the inlet (Channel 12) had the maximum flow velocity (i.e. 1.03 and 0.67 m/s for Type-2 and 3, respectively), but the flow velocity at Channel 1 was significantly lower (i.e. 0.26 and 0.06 m/s for Type-2 and 3, respectively). As a result, Types-2 and 3 cooling blocks always had a higher maximum CPV temperature compared to that of Type-1 (Figure 4.2). Moreover, this restriction in the flow distribution caused the high temperature regions on the CPV cells, as illustrated in Figures 4.4(b) and (c).

The same limitation was also noticed in Types-4 and 5 cooling blocks, where the outlet was located at the center. Rectangular fins in these two types blocked the coolant from flowing effectively to the outlet located at the center of the cooling block, as observed in Figures 4.3(d) and (e). As a result, the coolant flow velocity in the channels away from the outlet was lower. This reduction in coolant flow velocity had led to the reduction in the performance of forced convection between coolant and heat sink as the heat absorbed by

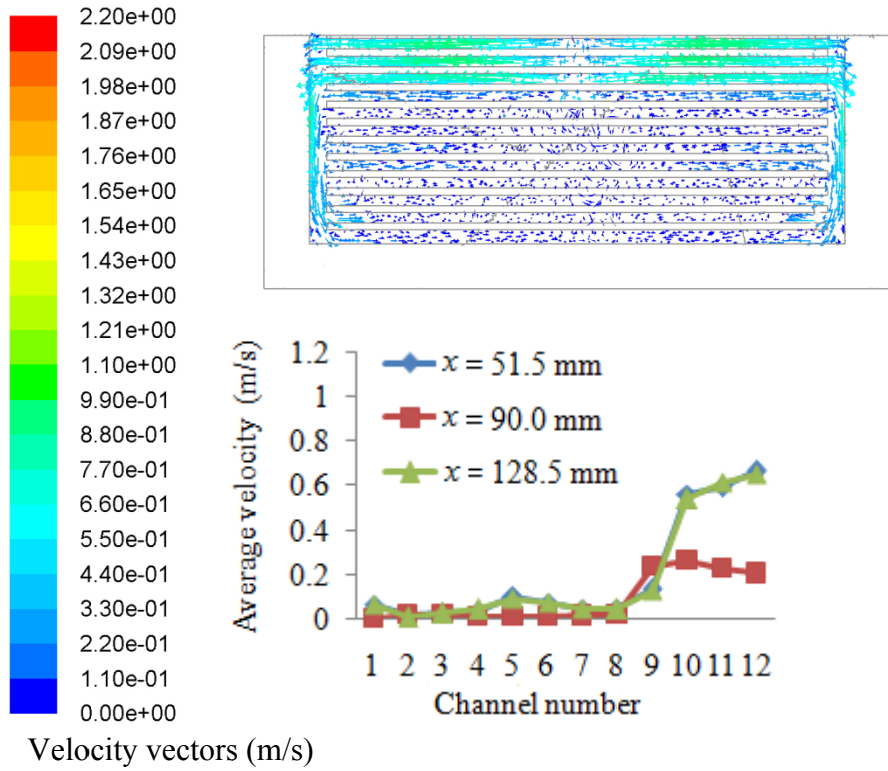
heat sink was unable to dissipate effectively to the coolant (Zhong et al., 2006; Zhong et al., 2007; Xie et al., 2009). Therefore, the CPV temperatures increased.



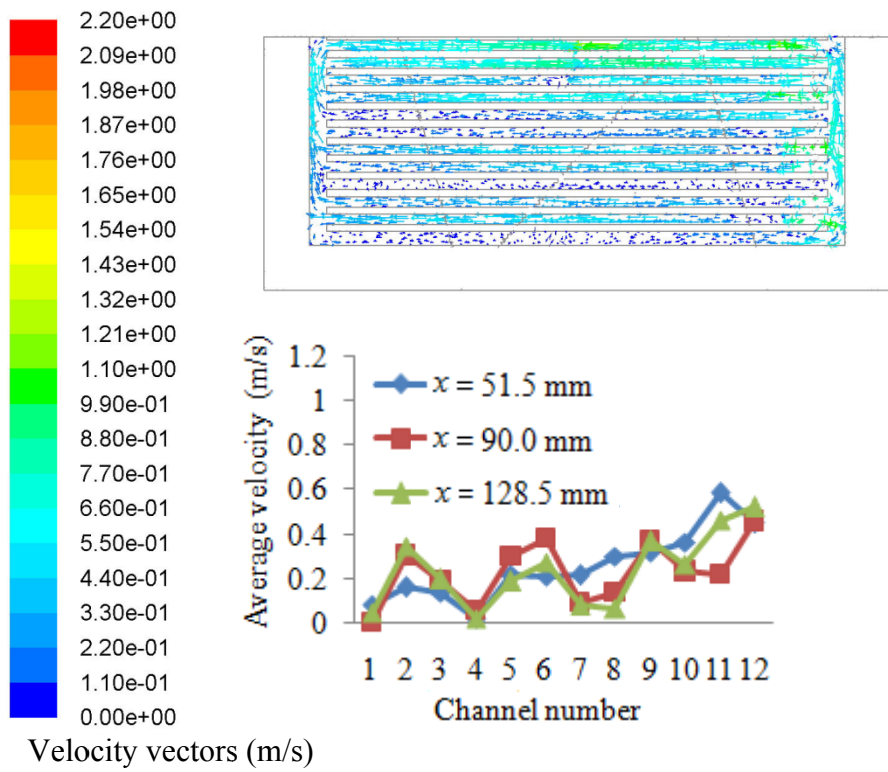
(a)



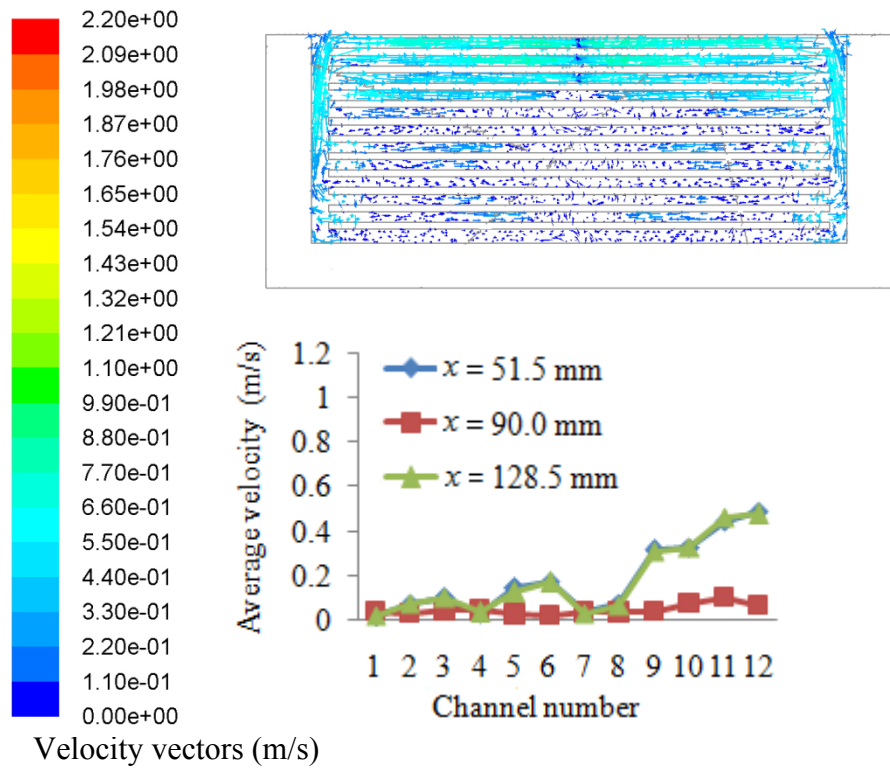
(b)



(c)

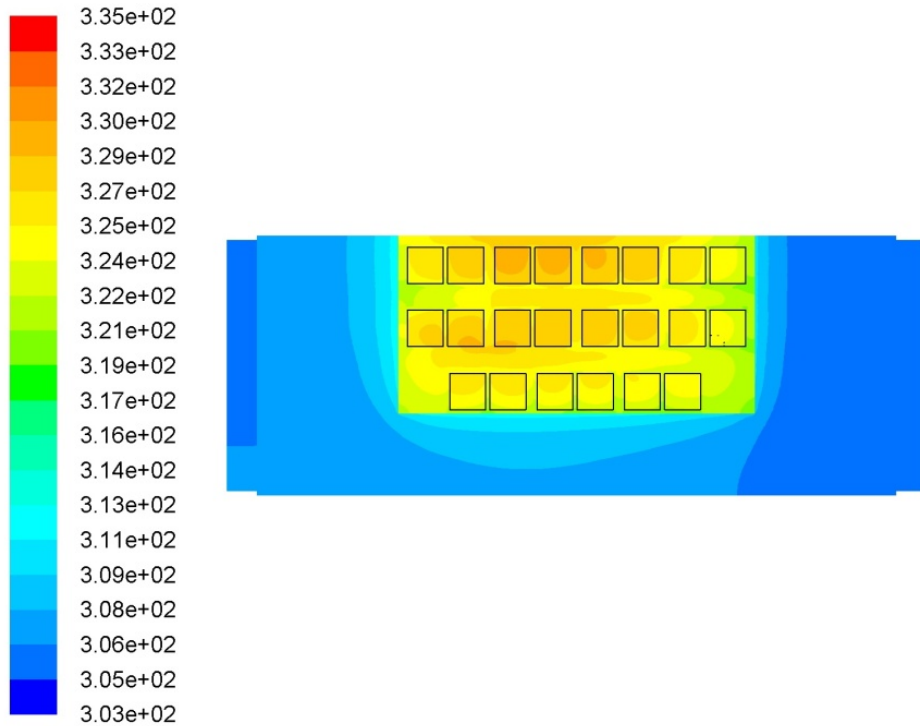


(d)



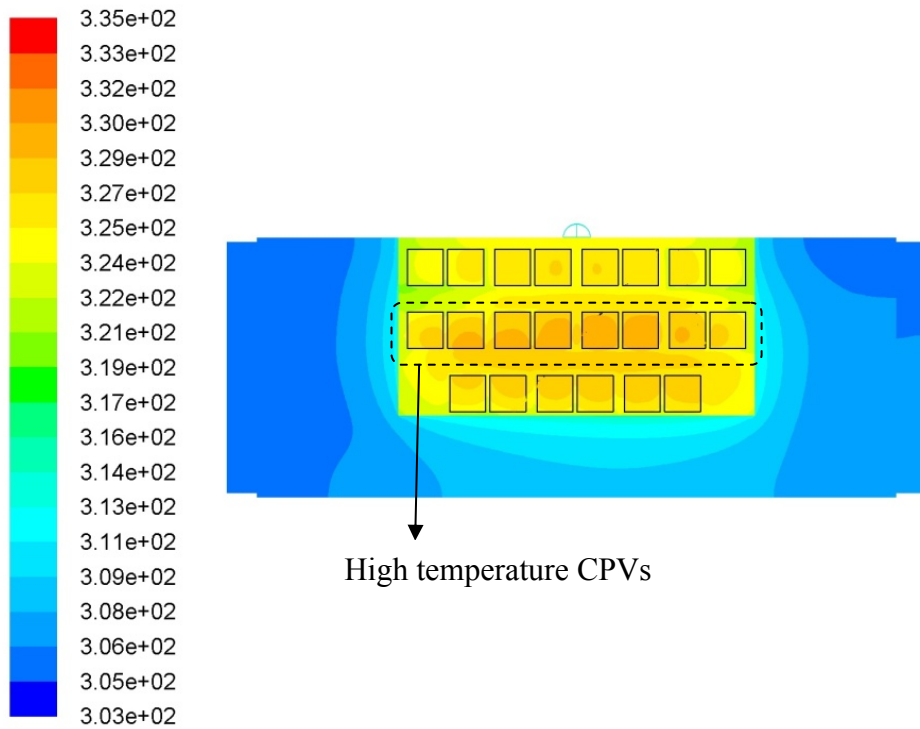
(e)

Figure 4.3: Middle-plane velocity vector fields and average velocity at different channel for (a) Type-1 (b) Type-2 (c) Type-3 (d) Type-4 and (e) Type-5 at a coolant flow rate of $4 \times 10^{-4} \text{ m}^3/\text{s}$



Contour of temperature (K)

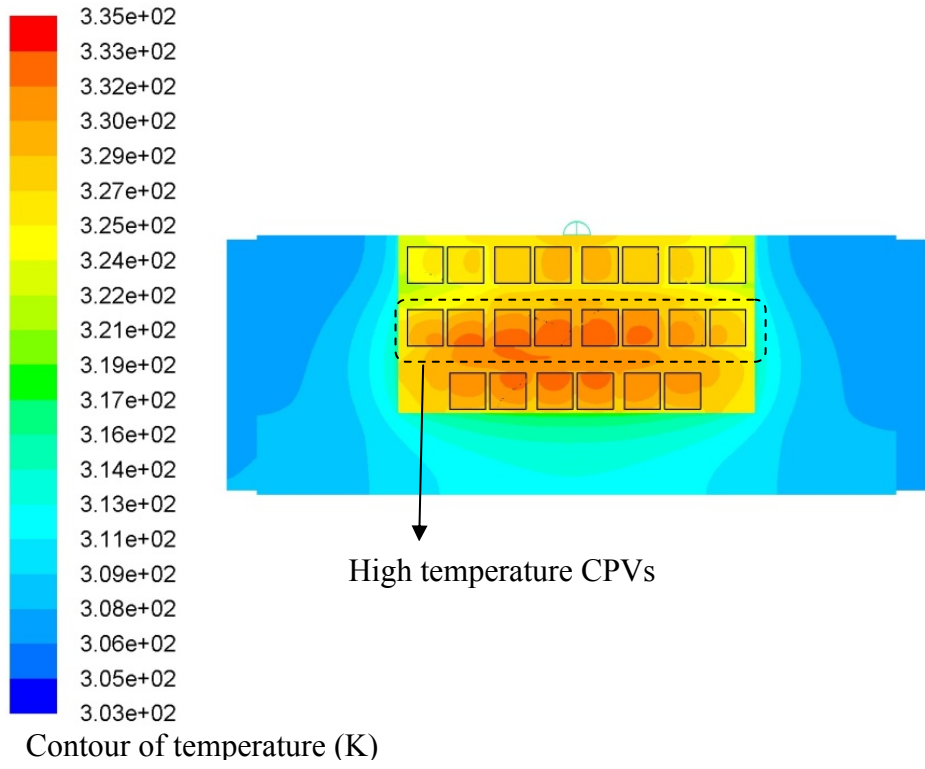
(a)



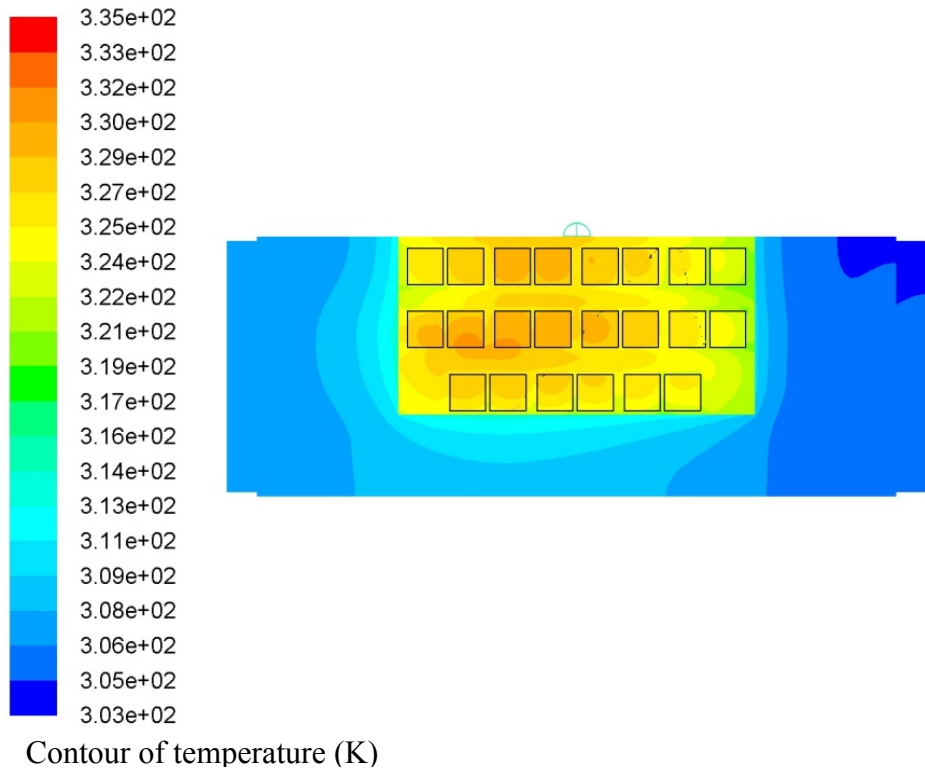
Contour of temperature (K)

High temperature CPVs

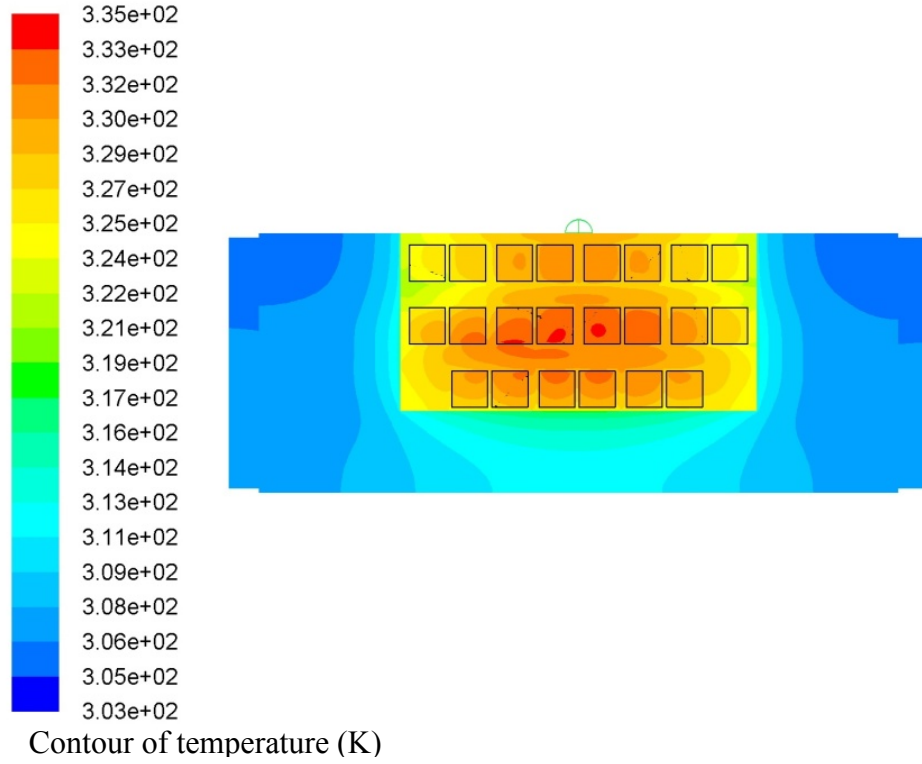
(b)



(c)



(d)



(e)

Figure 4.4: Temperature contours for (a) Type-1 (b) Type-2 (c) Type-3 (d) Type-4 and (e) Type-5

Figure 4.5 shows the normal distribution of CPV temperature, where the coolant flow rate was remained constant at $4 \times 10^{-4} \text{ m}^3/\text{s}$ for all five types of inlet/outlet arrangement. In Figure 4.5, x -axis represents the mean CPV temperature, while y -axis represents the probability density that was obtained from the probability density function for normal distribution

$$f(x) = \frac{1}{\sqrt{2\pi}\sigma} e^{-\frac{(x-\mu)^2}{(2\sigma^2)}} \quad (4.5)$$

where x is the CPV temperature (K), μ is the mean temperature (K) and σ is the standard deviation (K) of the CPV temperature. Probability density

function was used to plot the normal distribution curve (or bell curve) and to find the probability

$$P(a \leq X \leq b) = \int_a^b f(x)dx \quad (4.6)$$

where $P(a \leq X \leq b)$ is the probability that X falls in the interval of a and b (Devore, 2000).

It could be noticed that compared to other configurations, Type-1 cooling block had the minimum mean CPV temperature and a small standard deviation, suggesting that Type-1 had the best performance in achieving the temperature uniformity. Therefore, the multiple inlet/outlet design best worked with the rectangular fin cooling block without fin split as it allowed coolant to flow more evenly into each channels as presented in Figure 4.3(a). For Types-2 and 4 cooling blocks, the temperature standard deviations were close to that of Type-1, but with higher mean CPV temperatures. It was found that the rectangular fins restricted the coolant to flow and to distribute freely from the inlet (Type-2) or to the outlet (Type-4) (Figures 4.3(b) and (d)). As a result, the coolant flow velocity and therefore the convective heat transfer between the cooling block and coolant were decreased (Equation 2.3, 4.1, 4.2 and 4.3).

Types-3 and 5 cooling blocks exhibited the minimal cooling performance, possibly due to their larger inlet area, and leading to a lower inlet velocity. As a result, the rate of convective heat transfer between the cooling block and coolant was reduced leading to a higher standard deviation of CPV temperature and mean temperature. In addition, these two

configurations also had the same constraints in evenly distributing the flow, which had decreased the cooling performance (Figures 4.3(c) and (e)).

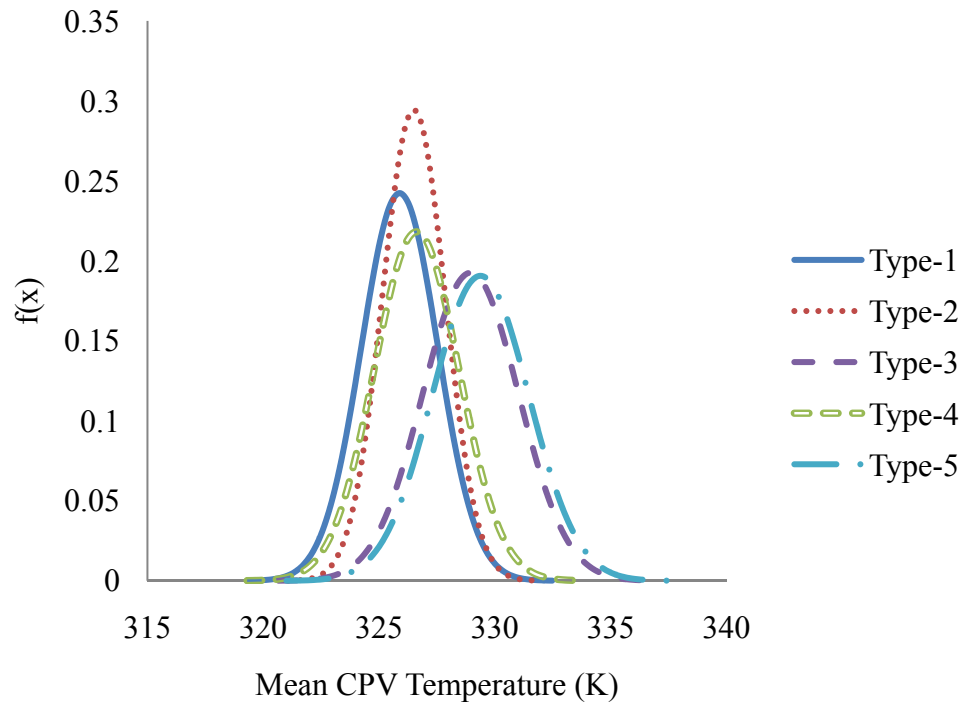


Figure 4.5: Effect of inlet/outlet arrangement on CPV temperature uniformity

4.3 Effect of Inlet Flow Rate (Case Study 2)

Figure 4.2 also shows the effect of inlet flow rate on the reduction of the CPV maximum temperature. By increasing the inlet flow rate from 4×10^{-4} to $12 \times 10^{-4} \text{ m}^3/\text{s}$, the CPV maximum temperature reduction of 4.04, 4.33, 4.63, 5.58 and 5.92 K for Types-1, 2, 3, 4 and 5, respectively, could be observed. Higher coolant flow rate leading to a lower thermal resistance between the cooling block and coolant was the possible reason for this phenomenon. As a result, more heat could be dissipated and the CPV temperature could be

reduced (Equation 2.3, 4.1, 4.2 and 4.3). However, this effect declined gradually as the flow rate increased. This finding agreed well with the works presented by Li et al. (2005) and Li et al. (2009). The influence of Reynolds number for impinging jet on heat sink was studied. It was found that thermal resistance of the heat sink was reduced gradually when the impinging Reynolds number was increased (i.e., higher flow rate). Li and Chen (2007) also concluded that when the Reynold number for a heat sink was increased from 5,000 to 10,000, 15,000, 20,000 and 25,000, the thermal resistance were reduced by 37.34 %, 22.43 %, 21.89 % and 4.94 % , respectively.

The effect of inlet flow rate on the CPV temperature uniformity for Type-1 cooling block is shown in Figure 4.6. It was again confirmed that the higher flow rate could improve the heat transfer between cooling block and coolant (Zhong et al., 2006; Zhong et al., 2007; Xie et al., 2009), leading to the better temperature uniformity. For instance, by increasing the inlet flow rate from 4×10^{-4} to 12×10^{-4} m³/s, a standard deviation reduction from 1.65 to 1.19 K could be observed.

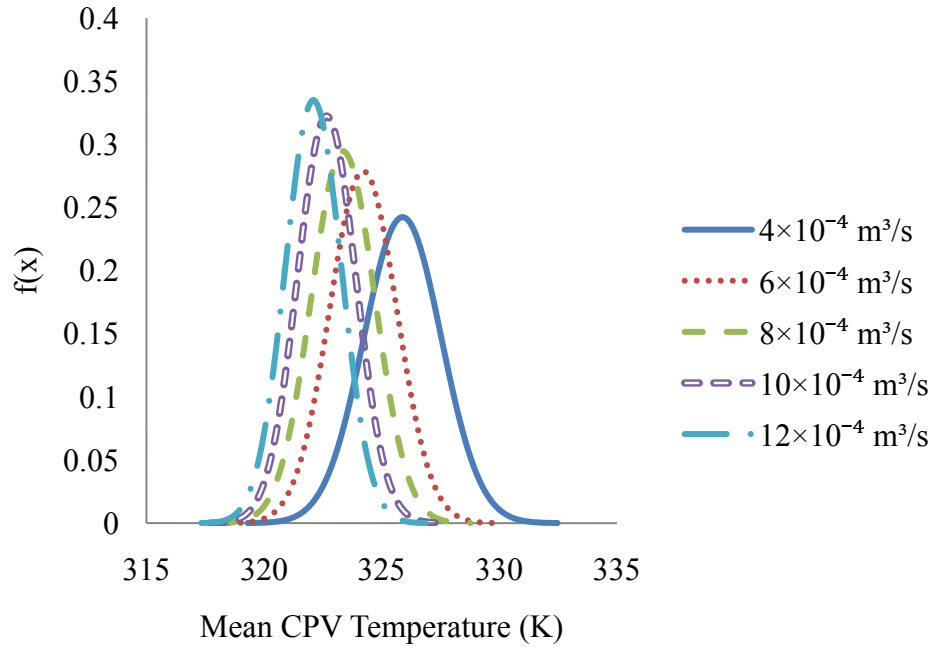


Figure 4.6: Effect of inlet flow rate on CPV temperature uniformity for Type-1 cooling block

4.4 Effect of Fin Split (Case Study 3)

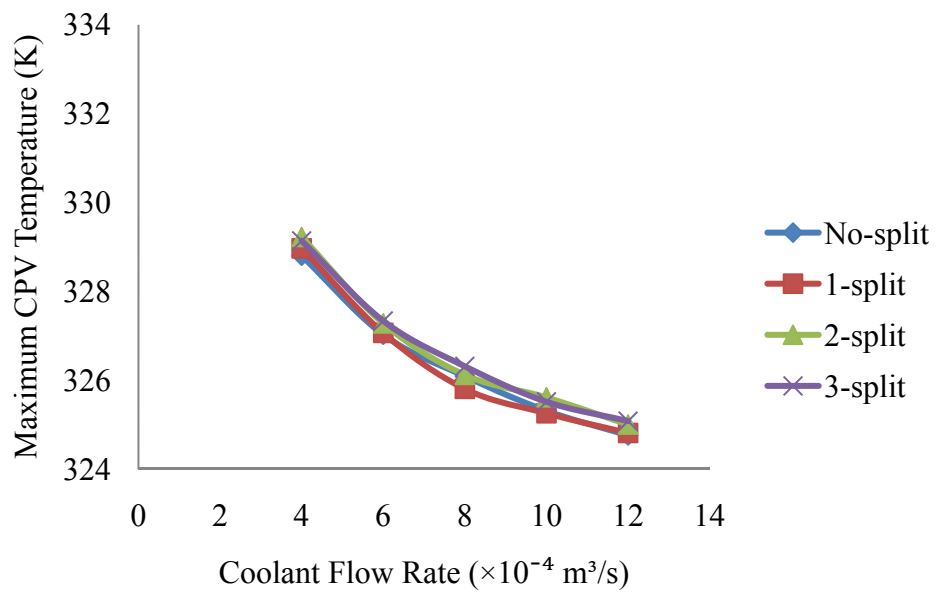
As depicted in Figure 4.7, it could be seen that in addition to inlets/outlets arrangement and flow rate, the fin split also had a great effect on cooling performance. The fin split had the most significant influence on Type-3. A maximum temperature difference of up to 2.94 K could be observed. On the other hand, the influence of fin split was lesser for Type-2, where maximum temperature difference was up to 0.77 K. The fin split had more significant impact on Types-2 and 3, which were both center jet impingement design (Figures 3.7(b) and (c), respectively) since the fin splits located at the middle allowed the inlet flow to distribute more effectively and evenly to other

channels and maintained a higher coolant flow velocity in the channels further away from the center of the heat sink (Figures 4.8(b) and (c)). This higher coolant flow velocity had led to the reduction in the thermal resistance between the heat sink and coolant (Zhong et al., 2006; Zhong et al., 2007; Xie et al., 2009), resulting in the reduction of the temperature of the CPV.

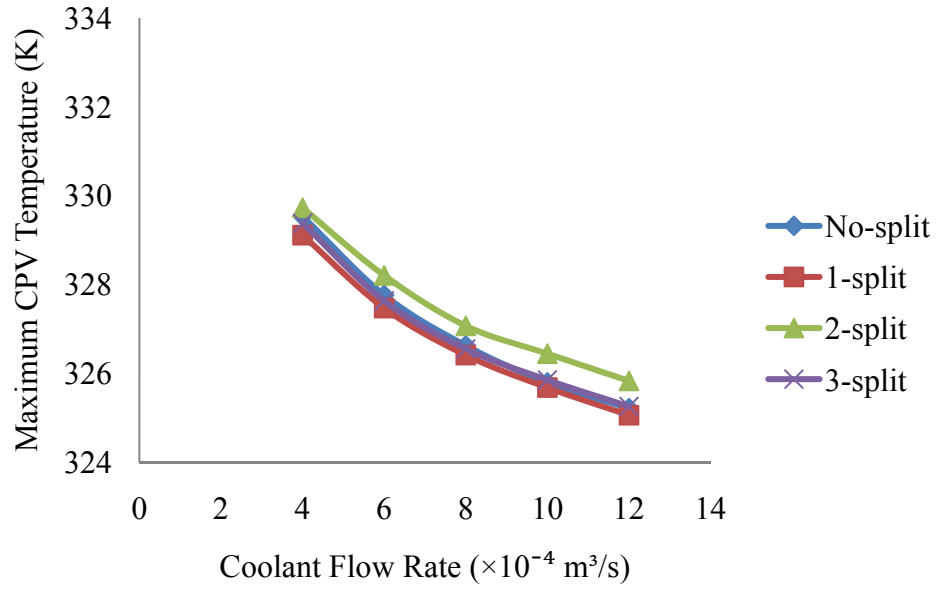
The fin split exhibited the least influence on Type-1, where a maximum temperature difference of up to 0.5 K was observed. As the positions of the inlets and outlets were located at two sides for Type-1, most of the coolant flow was restricted to flow horizontally, which was from right to left in this case (Figure 4.8(a)). Hence, the introduction of the fin split was not as effective as the center jet impingement design was.

The number of fin split (and in turn the split location) also affected the cooling performance. Figures 4.7(b) and (c) showed that 1-split design had a better cooling performance with lowest maximum CPV temperature for Type-2 and 3. As observed in Figures 4.8(b) and 4.9 (b), both 1-split and 3-split designs allowed the coolant to enter the cooling block from the center to readily direct their flows to the surrounding channels. Based on Equation 2.3, it could be observed that the area for heat transfer was linearly proportional to convective heat transfer. Hence, 3-split design was determined to have a comparatively lower cooling performance because the total area for convective heat transfer was reduced as more fin splits were introduced. As for 2-split design, where fin splits were not located at the middle, a minimal performance was found as the coolant was unable to flow effectively to the

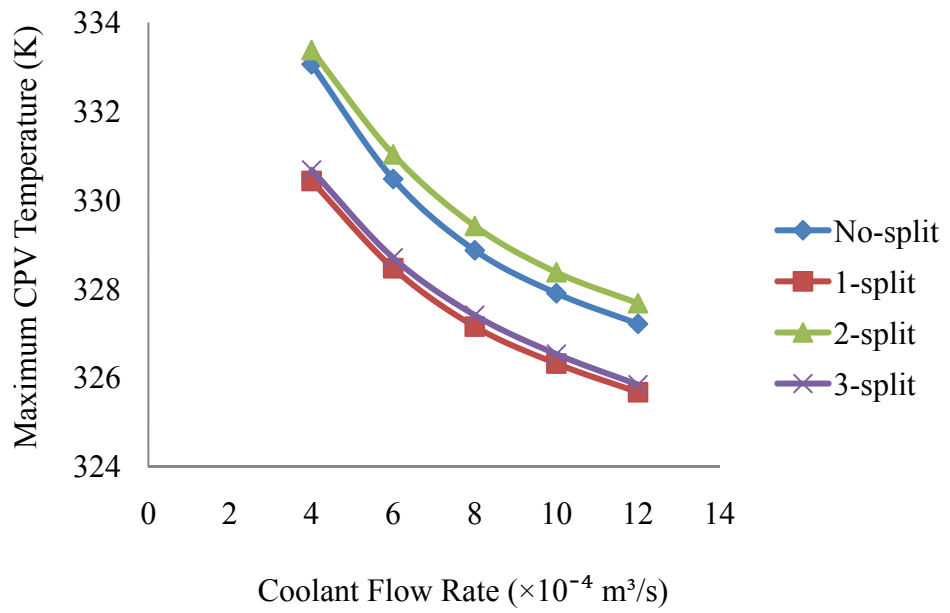
surrounding channels. This could be confirmed in Figure 4.9(a) that only a fraction of coolant flowed in the fin split channels. This flow resistance due to the blockage of the fins restricted the convective ability of the heat sink and resulted in a higher thermal resistance (Li et al., 2005). Hence, the CPV temperature for 2-split design was the highest among the three cases.



(a)

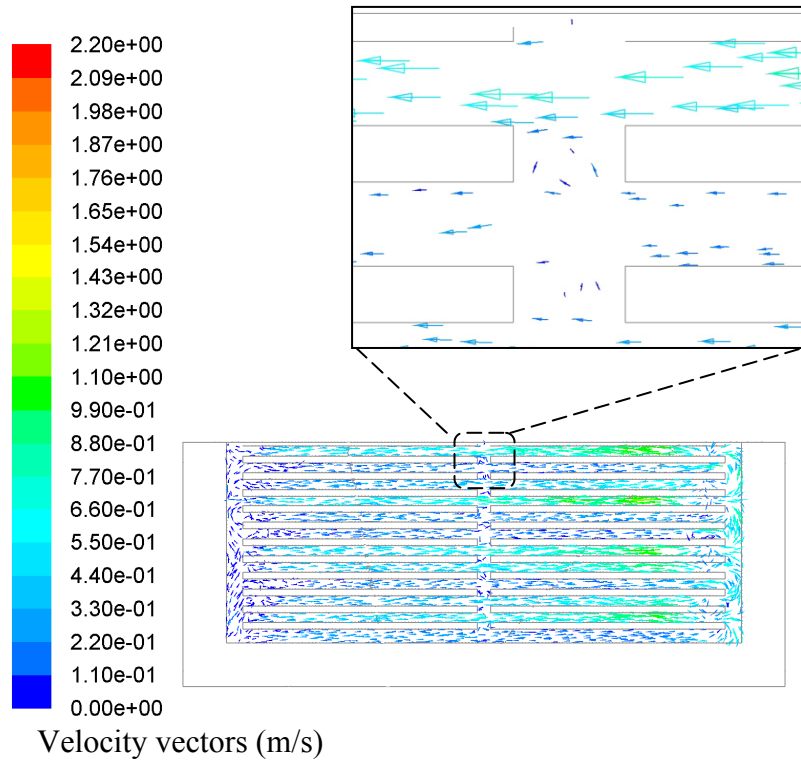


(b)

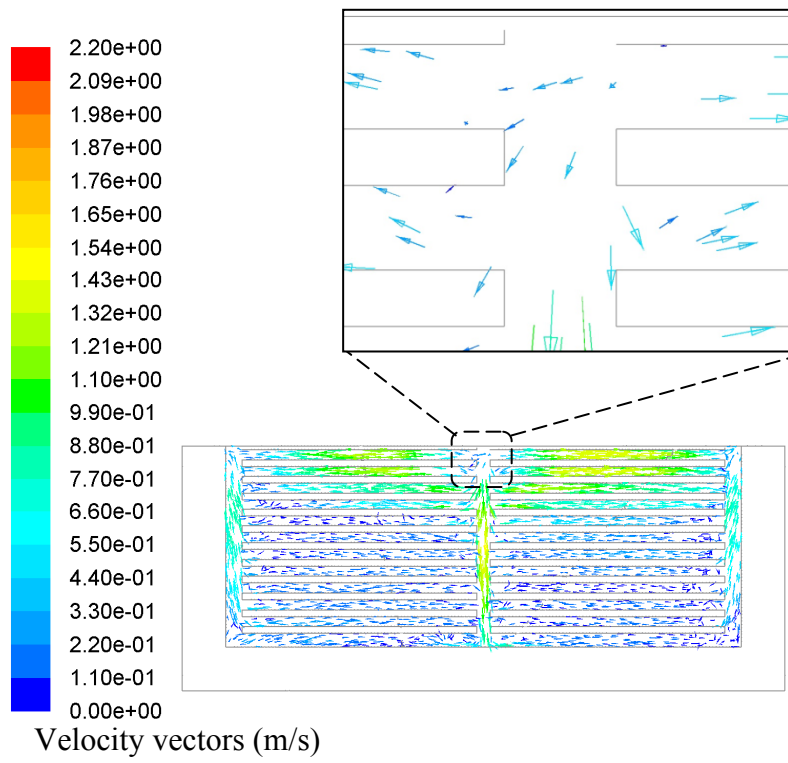


(c)

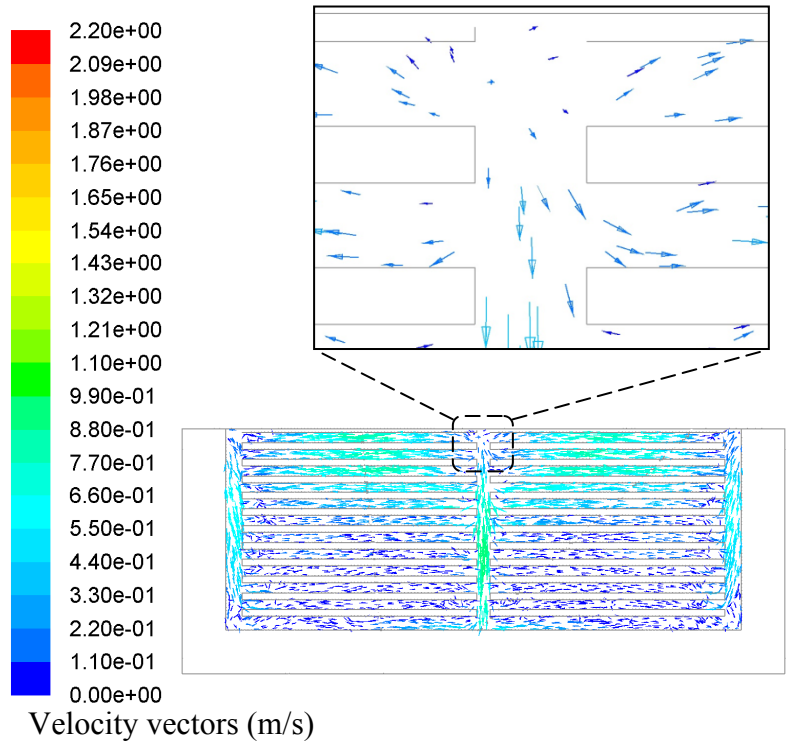
Figure 4.7: Effect of fin split on maximum CPV temperature for (a) Type-1 (b) Type-2 and (c) Type-3



(a)



(b)



(c)

Figure 4.8: Velocity vector fields for (a) Type-1(b) Type-2 and (c) Type-3 1-split design at a coolant flow rate of $4 \times 10^{-4} \text{ m}^3/\text{s}$

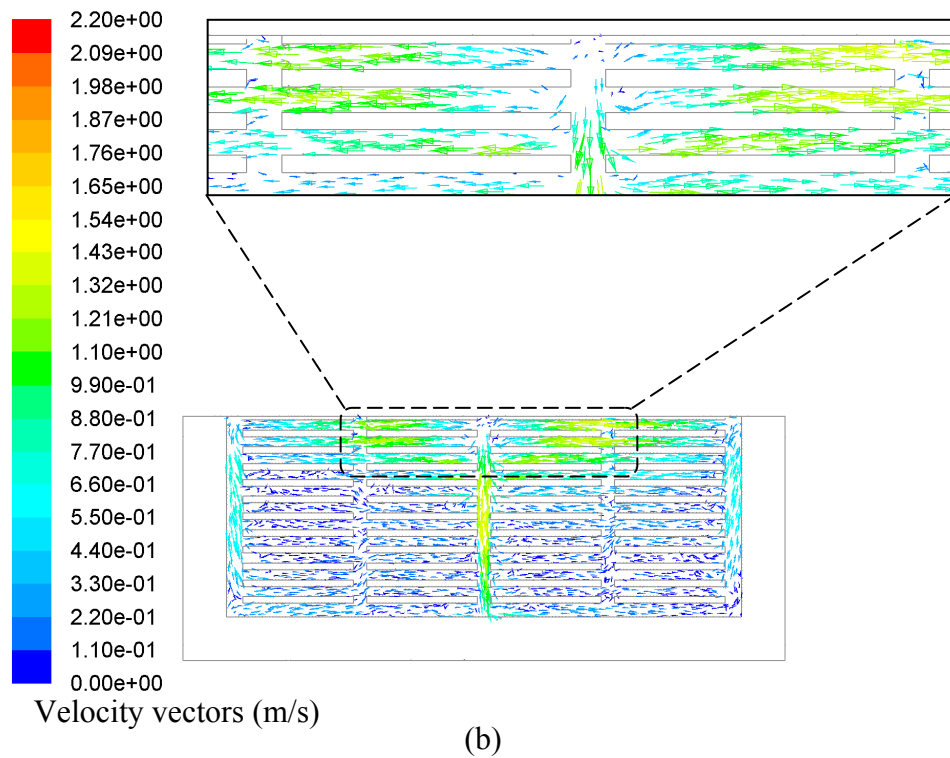
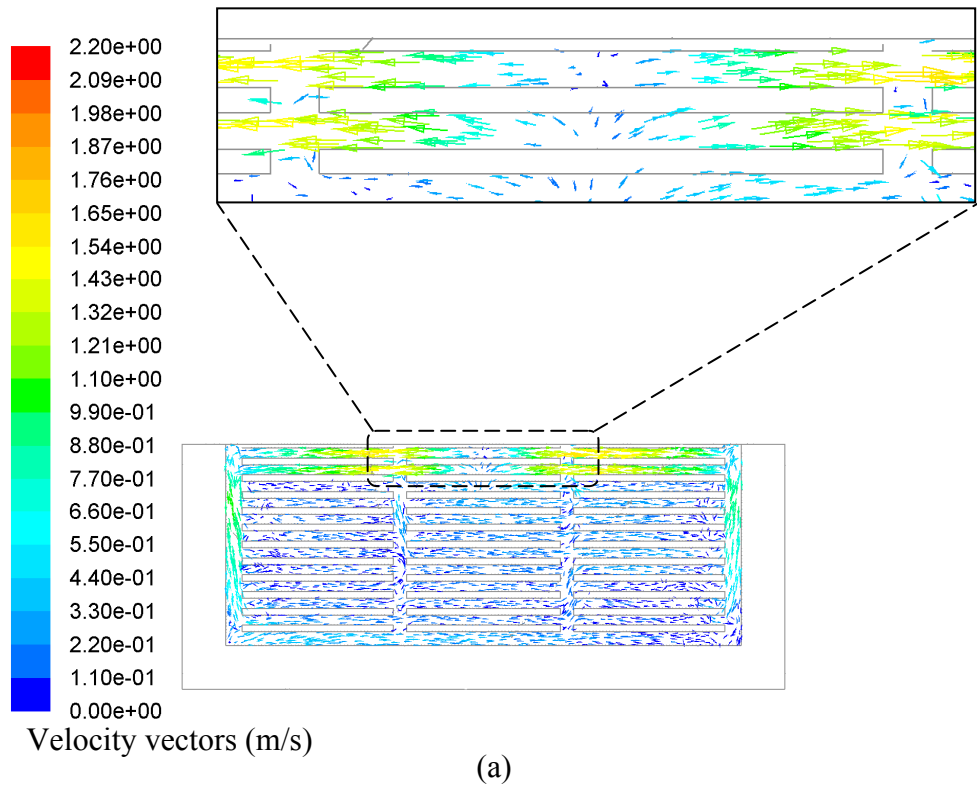
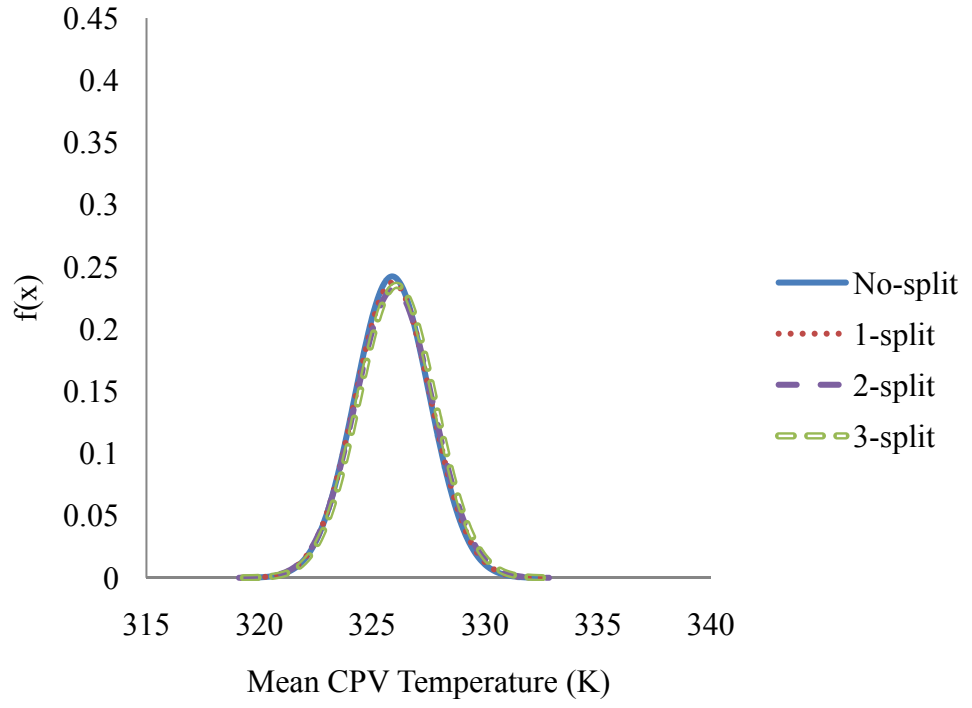


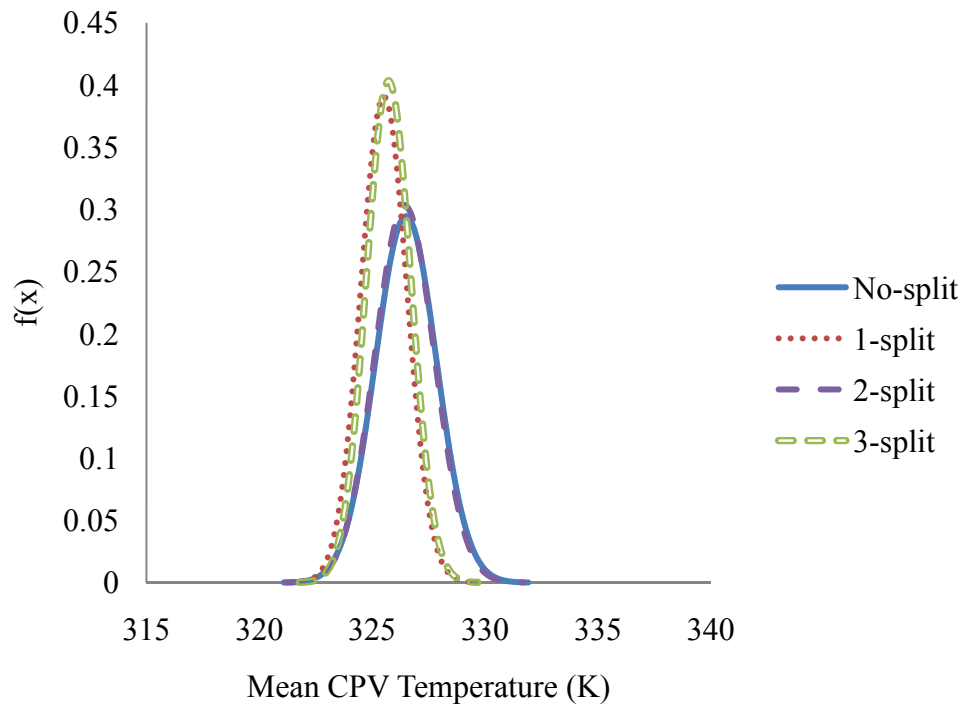
Figure 4.9: Velocity vector fields for Type-2 (a) 2-split and (b) 3-split cooling blocks at a coolant flow rate of $4 \times 10^{-4} \text{ m}^3/\text{s}$

Figure 4.10 presents the effect of fin split on the temperature uniformity of CPV, where the coolant flow rate was remained constant at $4 \times 10^{-4} \text{ m}^3/\text{s}$ for all three types of cooling blocks. In Figure 4.10, Type-2 and 3 were able to obtain a better temperature uniformity performance with fin designs of 1-split and 3-split. It might be due to the fact that the jet impingement at the center was able to distribute the flow effectively to the surrounding channels, significantly cooling the region with the highest temperature, which was located at the center of the cooling block (Figures 4.8(b) and 4.9(b)).

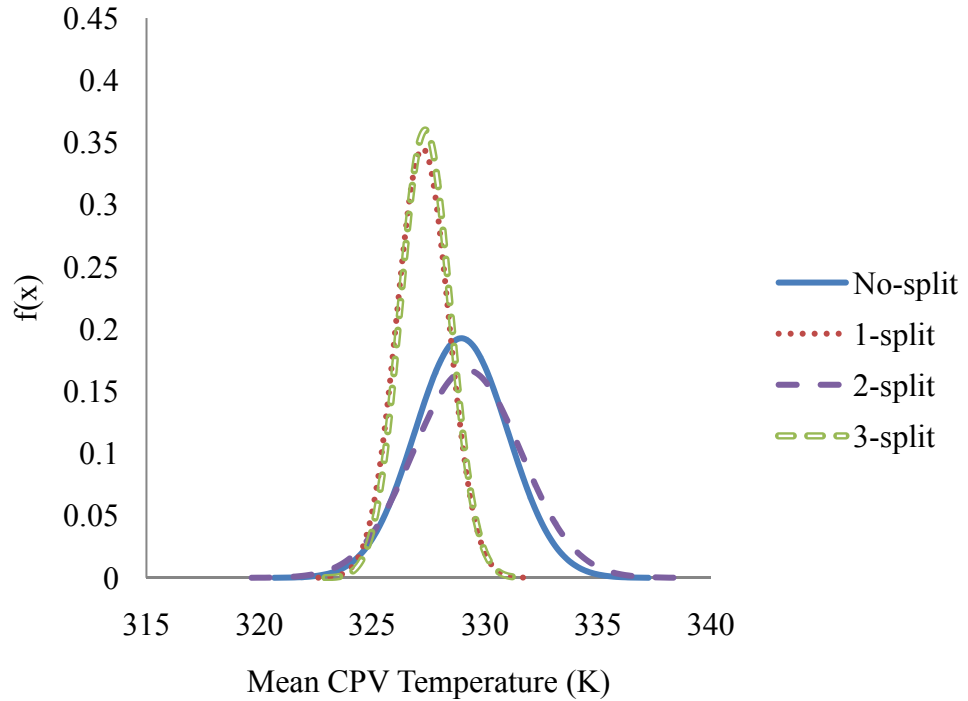
Comparisons were made by calculating the difference between the maximum and minimum mean CPV temperature of each fin split design for all cooling blocks. The same comparisons were made for standard deviation as well. It could be noticed that the fin split had the least influence on Type-1, where the difference on mean CPV temperature and standard deviation were only 0.19 and 0.07 K, respectively. Type-2 had the intermediate result, where the differences on mean CPV temperature and standard deviation were 0.98 and 0.37 K, respectively. The fin split had the greatest influence on Type-3, achieving 1.97 and 1.28 K on mean CPV temperature and standard deviation, respectively.



(a)



(b)



(c)

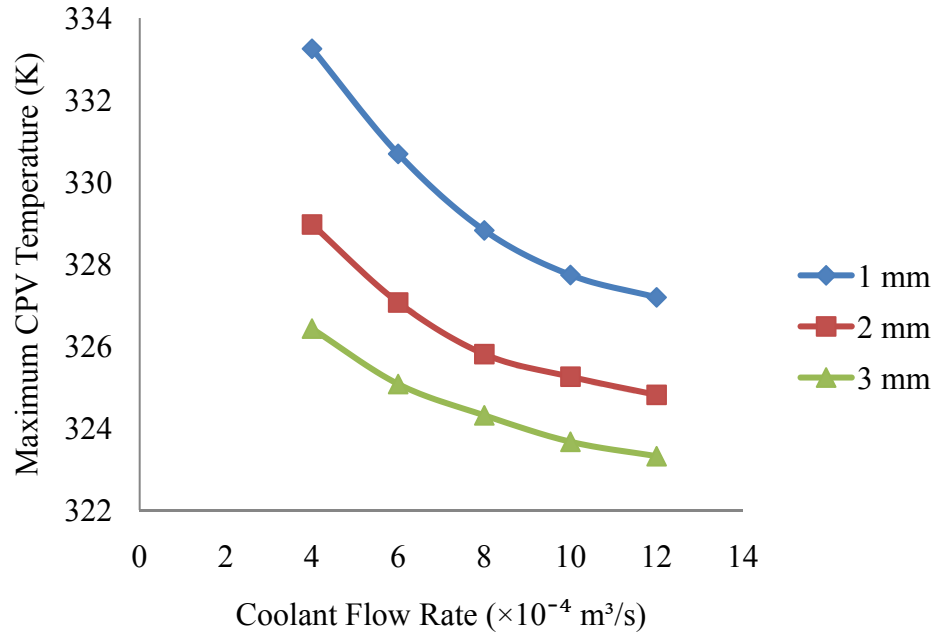
Figure 4.10: Effect of fin split on CPV temperature uniformity for (a) Type-1
(b) Type-2 and (c) Type-3 cooling blocks

4.5 Effect of Fin Width (Case Study 4)

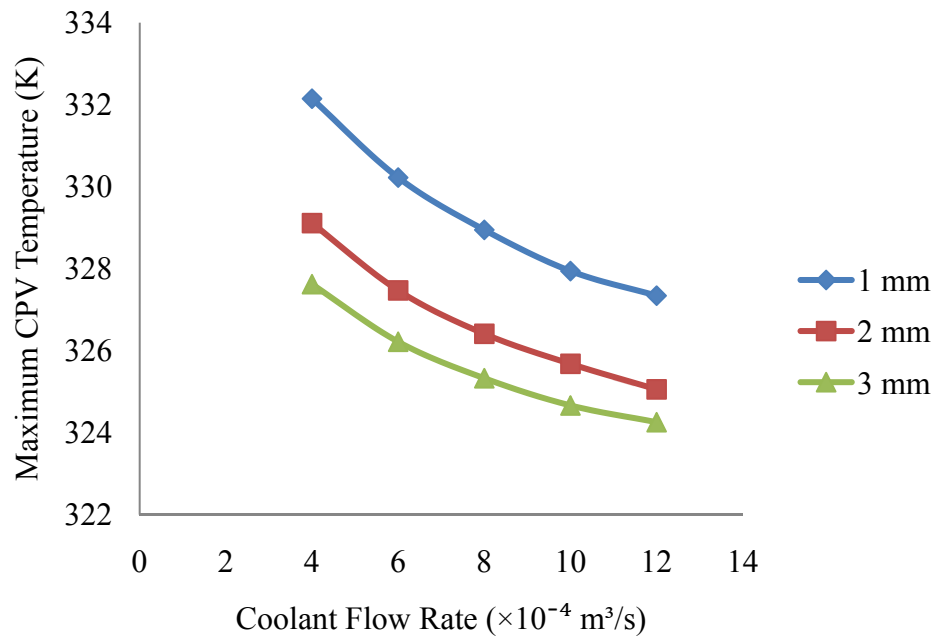
In this case study, the total number of fins in the cooling blocks ($n = 23$) and the length of the cooling block ($L_h = 180$ mm) were fixed in order to study the effect of fin width on maximum temperature and temperature uniformity of CPV. Due to these limitations, the fin width of up to 3 mm was used as further increment in the fin width required a reduction in number of fins or increment of length of cooling block.

Figure 4.11 illustrates the effect of the fin width on maximum CPV temperature for Types-1, 2 and 3 with 1-split fin. It could be noticed that the larger fin width had led to a better cooling performance for all three types of cooling blocks. For instance, at the coolant flow rate of $4 \times 10^{-4} \text{ m}^3/\text{s}$, increasing the fin width from 1 to 3 mm could reduce the maximum temperature by 6.83, 4.52 and 4.51 K for Types-1, 2, and 3, respectively. This finding indicated that the wider fin width provided larger heat transfer area to enhance the forced convection between the cooling block and incoming flow (Equation 2.3). Similar works had been conducted by Li and Chen (2007) and Li et al. (2005) where the effect of fin width on heat sink with impinging jet was studied and good agreement could be observed between the current and their studies. The results showed heat sink with a wider fin width had a larger area for heat transfer between the heat sink and impinging jet. As a result, the thermal resistance could be reduced effectively.

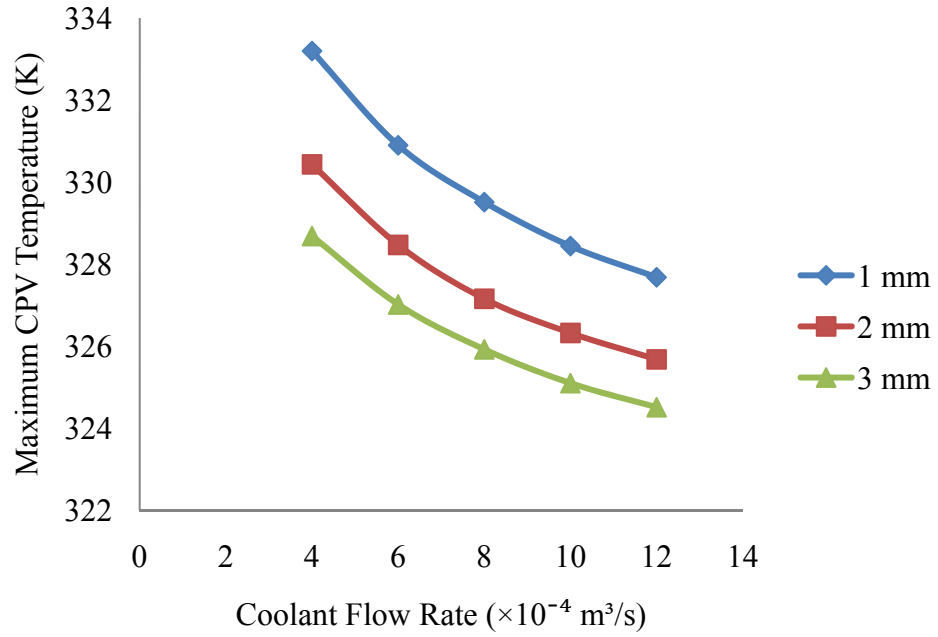
Besides, it could be observed from Figure 4.11 that the effect of fin width was especially important at a lower flow rate as this effect decreased gradually when the coolant flow rate increased. When the coolant flow rate was three times ($12 \times 10^{-4} \text{ m}^3/\text{s}$) compared to the earlier case, increasing the fin width from 1 to 3 mm could only reduce the maximum CPV temperature by 3.87, 3.09 and 3.17 K for Types-1, 2, and 3, respectively. This implies that the lower coolant flow rate for the smaller fin width was insufficient to encourage effective forced convection to cool the CPV.



(a)



(b)



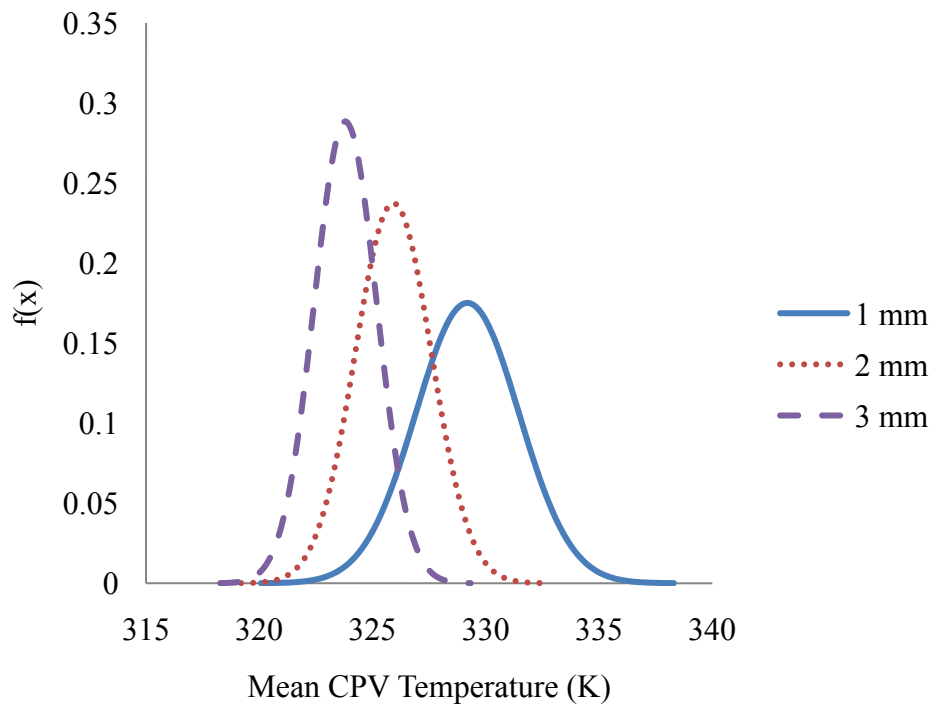
(c)

Figure 4.11: Effect of fin width on maximum CPV temperature for (a) Type-1
(b) Type-2 and (c) Type-3

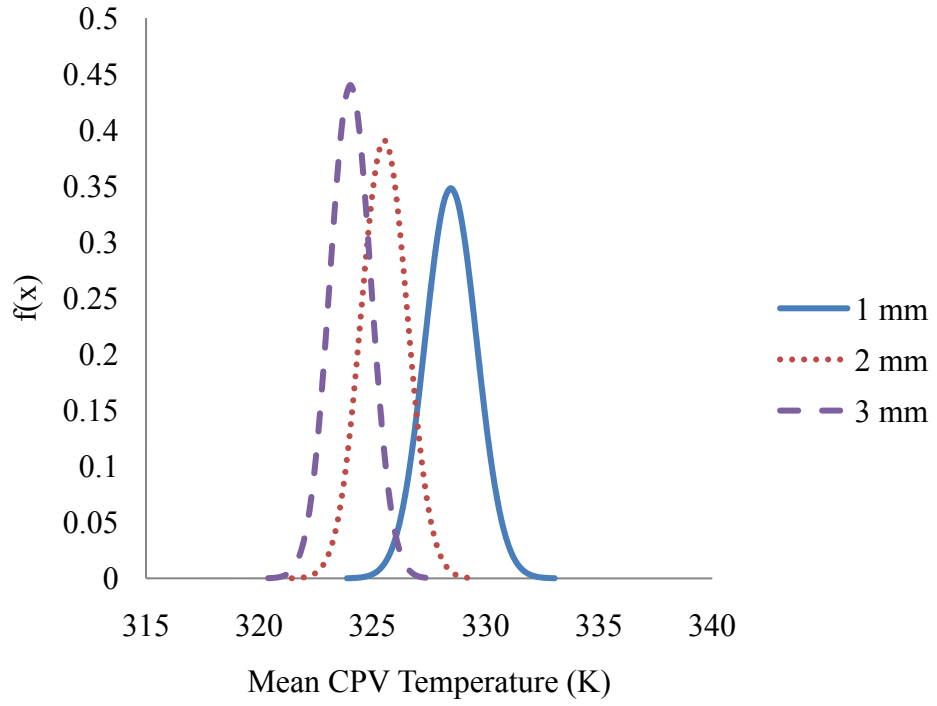
The effect of the fin width on the CPV temperature uniformity for Types-1, 2 and 3 cooling blocks is depicted in Figure 4.12. The coolant flow rate was remained constant at $4 \times 10^{-4} \text{ m}^3/\text{s}$ for all three types of cooling blocks in the numerical calculations.

It could be noticed that the increase in the fin width was able to reduce the mean CPV temperature and achieve a better temperature uniformity for all three designs of cooling blocks. The difference between the maximum and minimum mean CPV temperature of each design was calculated for comparison. Of the three designs, the influence of fin width on Type-1 was the most significant, where the mean CPV temperature and standard deviation difference were 5.38 and 0.90 K, respectively. Type-2 had the intermediate

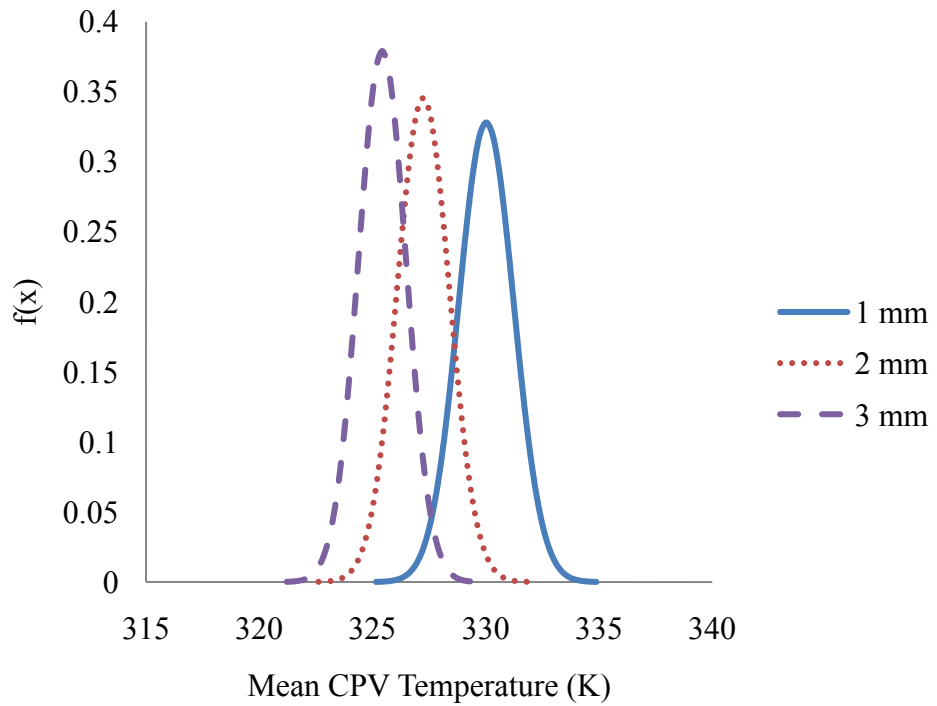
result, where the mean CPV temperature difference and standard deviation were 4.44 and 0.24 K, respectively. Nevertheless, the influence on Type-3 was the least, showing a mean CPV temperature and standard deviation differences of 4.59 and 0.16 K, respectively. This might be due to the fact that increment in the fin width led to a larger heat transfer area for forced convection (Li et al., 2005; Li and Chen, 2007). As a result, a better thermal uniformity could be achieved.



(a)



(b)



(c)

Figure 4.12: Effect of fin width on CPV temperature uniformity for (a) Type-1

(b) Type-2 and (c) Type-3 cooling blocks

4.6 Effect of Fin Spacing (Case Study 5)

In order to study the effect of fin spacing on maximum temperature and temperature uniformity of CPV, the computations were conducted with fixed length of cooling block ($L_b=180$ mm) and fin width ($W_f=2$ mm).

Figure 4.13 illustrates the effect of fin spacing on the cooling performance of cooling block at varied inlet flow rates. It could be seen that the maximum CPV temperature could be reduced by decreasing the fin spacing. This was probably due to the fact that a reduction in fin spacing had led to an increment in the total number of fins in the cooling block. As a result, the total area for forced convective heat transfer was increased and the thermal resistance between the cooling block and coolant was reduced (Equation 2.3). However, this trend was less significant with increasing inlet flow rate. For instance, at 4×10^{-4} m³/s, by reducing the fin spacing from 4 to 2 mm, a reduction of 2.89 K in maximum CPV temperature could be achieved. On the other hand, the temperature reduction was only 1.51 K at the flow rate of 12×10^{-4} m³/s. In this case, when the coolant flow rate was three times, only about 50 % reduction could be observed. This was due to the fact that increase in convective heat transfer area and inlet flow rate could only reduce the convective thermal resistance. As total thermal resistance consisted of both convective and conductive thermal resistance, the conductive thermal resistance became more important when the convective thermal resistance was reduced. Therefore, the influence of reduction in the convective thermal

resistance on the cooling performance was minimized, resulting in a smaller temperature reduction.

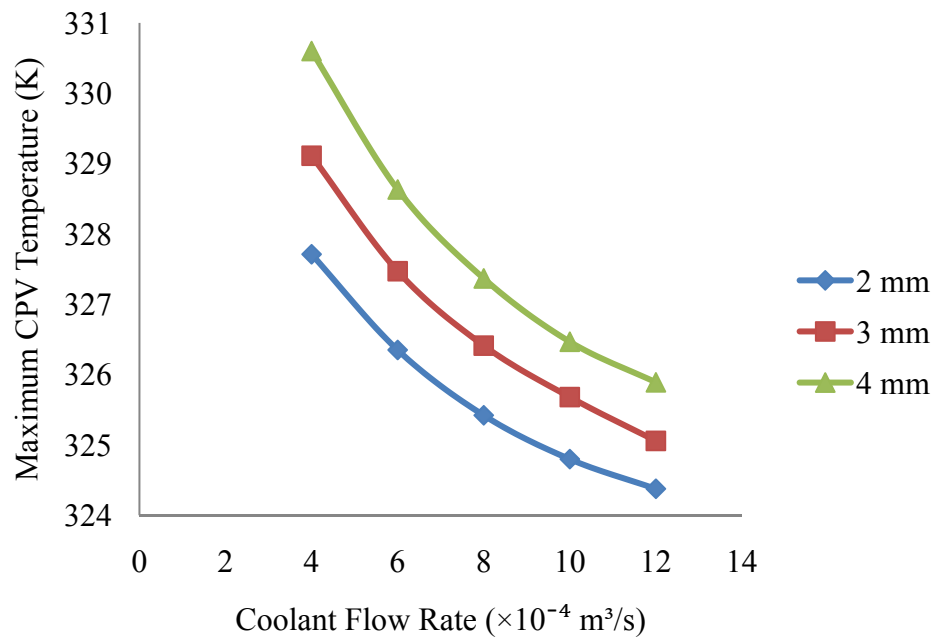


Figure 4.13: Effect of fin spacing on maximum CPV temperature

Figure 4.14 depicts the effects of fin spacing on the CPV temperature uniformity. The computations were conducted for the case of constant coolant flow rate of $4 \times 10^{-4} \text{ m}^3/\text{s}$.

It could be learned from Figure 4.14 that increasing the fin spacing had resulted in a higher mean CPV temperature and standard deviation, implying a poorer performance in thermal uniformity. This was a result of lower convective heat transfer area and therefore a lower forced convective heat transfer between the cooling block and the coolant when the number of fins was reduced.

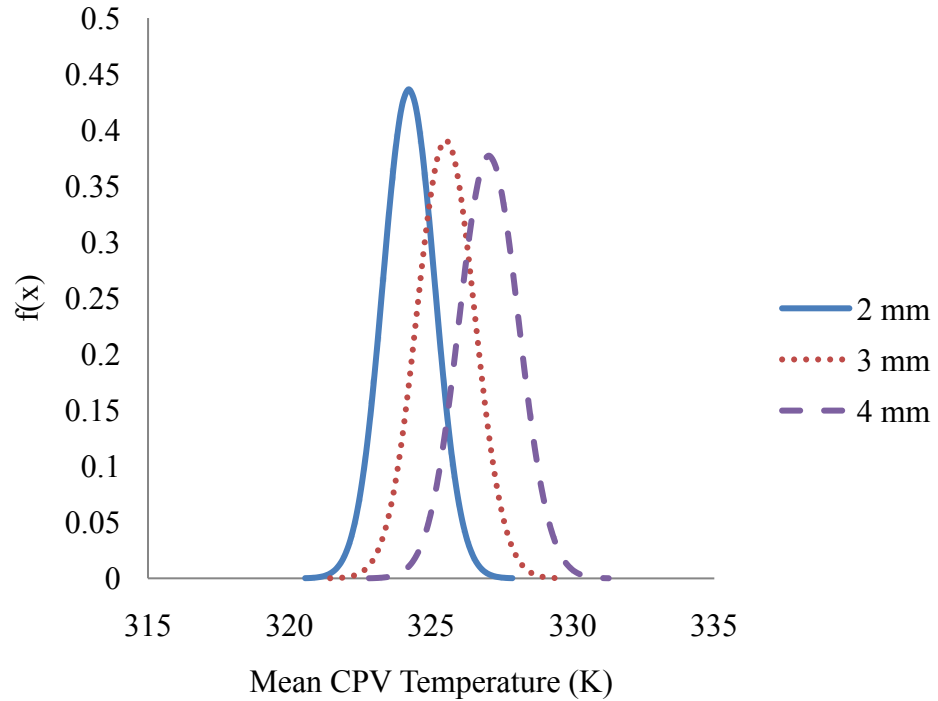


Figure 4.14: Effect of fin spacing on CPV temperature uniformity

4.7 Effect of Inlet/Outlet Area Ratio (Case Study 6)

When inlet/outlet area ratio was the focus of study, all dimensions of cooling blocks and fins used in the numerical computations were fixed according to Type-2 design with 1-fin split. Changes were made by varying the size of inlet area. Three inlet/outlet area ratios used in the study were 0.5, 1.0 and 1.5. The results of computations are plotted in Figure 4.15.

Compared to the case where inlet/outlet area ratio equalled to 1.0, it could be observed that a 50% reduction in inlet area (inlet/outlet area ratio = 0.5) had resulted in a reduction in the maximum CPV temperature of up to

0.84 K (Figure 4.15). On the other hand, a maximum temperature increment of up to 0.45 K could be observed when the inlet/outlet area ratio was 1.5.

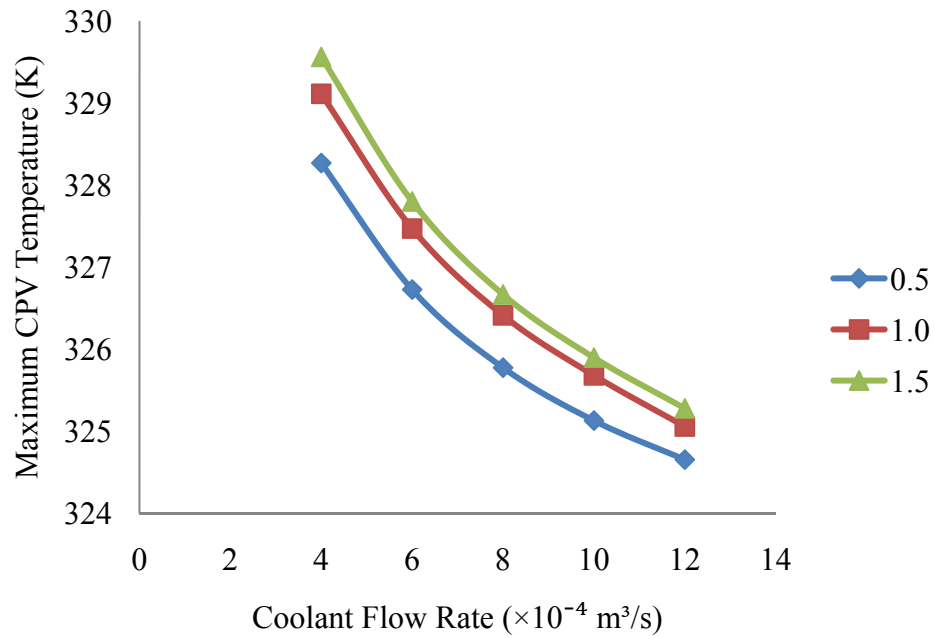


Figure 4.15: Effect of inlet/outlet area ratio on maximum CPV temperature

The effect of inlet/outlet area ratio on the CPV temperature uniformity could be viewed in Figure 4.16. It could be noticed that lowering the inlet/outlet area ratio had improved the thermal uniformity of the cooling block.

The reduction in maximum CPV temperature and better temperature uniformity might be attributed to the fact that a lower inlet area had led to a higher inlet velocity as the coolant flow rate was remained constant, which could be calculated using Equation 4.5

$$Q = Av \tag{4.7}$$

where Q is the volumetric flow rate (m^3/s), A is the inlet area (m^2) and v is the inlet velocity. As higher inlet velocity led to a better convective heat transfer, the cooling performance was improved (Li et al., 2005; Li and Chen, 2007; Li et al., 2009).

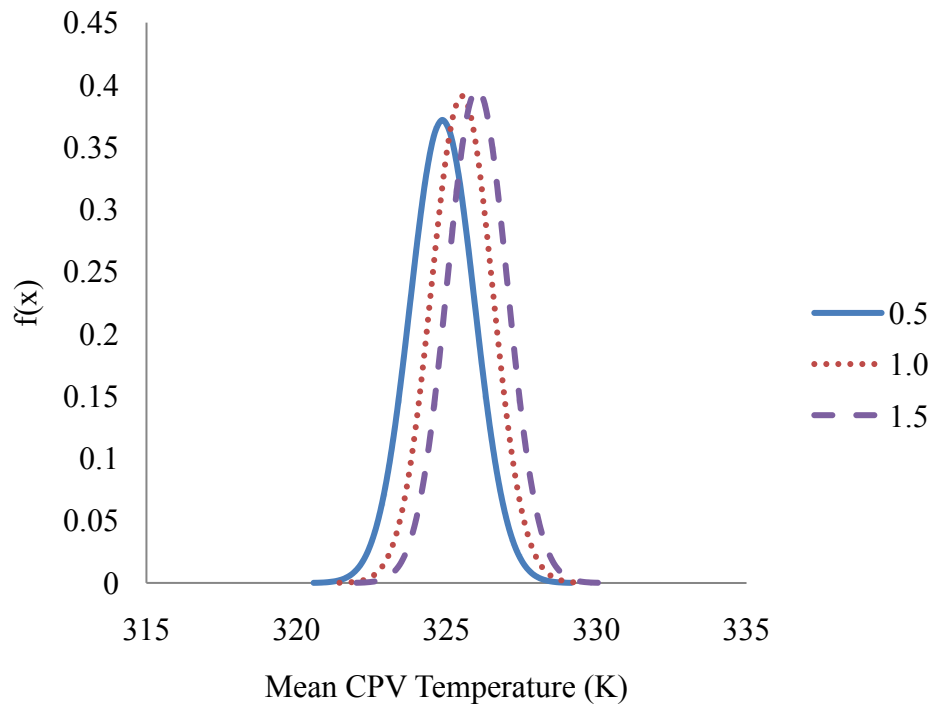


Figure 4.16: Effect of inlet/outlet area ratio on CPV temperature uniformity

4.8 Effect of Fin Height (Case Study 7)

In the case study for effect of fin height on maximum temperature and temperature uniformity of CPV, cooling block's geometrical parameters and fin design were fixed as per Type-2 with 1-fin split, except the heights of fins. Three fin heights, which were 10, 15 and 20 mm were used in the computations. The results are plotted in Figure 4.17.

As shown in Figure 4.17, the taller fins generally demonstrated slightly lower cooling performance (i.e., higher maximum CPV temperature). The reason was possibly due to the fact that increasing the fin height resulted in increased total area for heat transfer in the higher region. As this higher region was located at a longer distance from the heat source, the temperature was lower, resulting in smaller convective heat transfer which is a function of temperature difference. Moreover, increase in fin height also provided larger channel area for water flow, leading to lower flow velocity in channels, assuming that the volumetric water flow rate remained constant. As a result, the convective heat transfer was reduced and resulted in a lower cooling performance.

The influence of fin height on the cooling performance was not as significant as the results presented by Li et al. (2005), Li and Chen (2007) and Li et al. (2009). It should be noted that air-cooled system in which air was chosen as coolant was used in their works. The system was not enclosed and air was able to flow freely to higher fins. However, water was selected as coolant in this study due to higher thermal conductivity. But, water-cooled system must be enclosed to prevent the moisture from damaging the electronics components. As a result, the water flowed less freely, and hence the effect of fin height on cooling performance was less significant in this study.

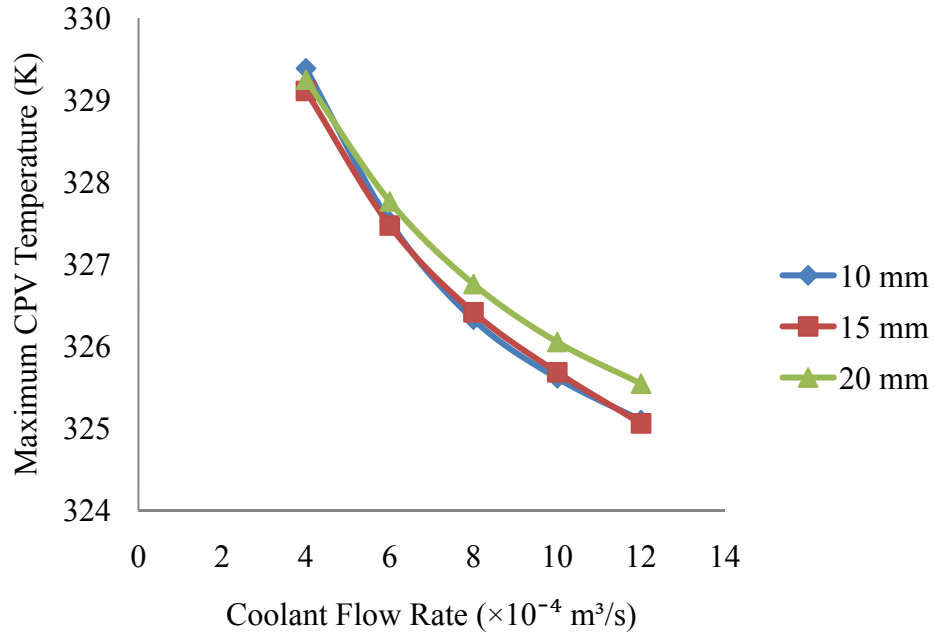


Figure 4.17: Effect of fin height on maximum CPV temperature

Figure 4.18 plots the effect of fin height on the temperature uniformity. The numerical results also indicated that increasing the fin height had slightly improved the thermal uniformity of the CPV. For instance, by increasing the fin height from 10 to 20 mm, the standard deviation could only be improved by 0.1 K. However, increment in fin height also resulted in a higher mean CPV temperature. For instance, an increment of 0.3 K could be noticed by increasing the fin height from 10 to 30 mm. Hence, it could be concluded that the influence of fin height on cooling performance was less important.

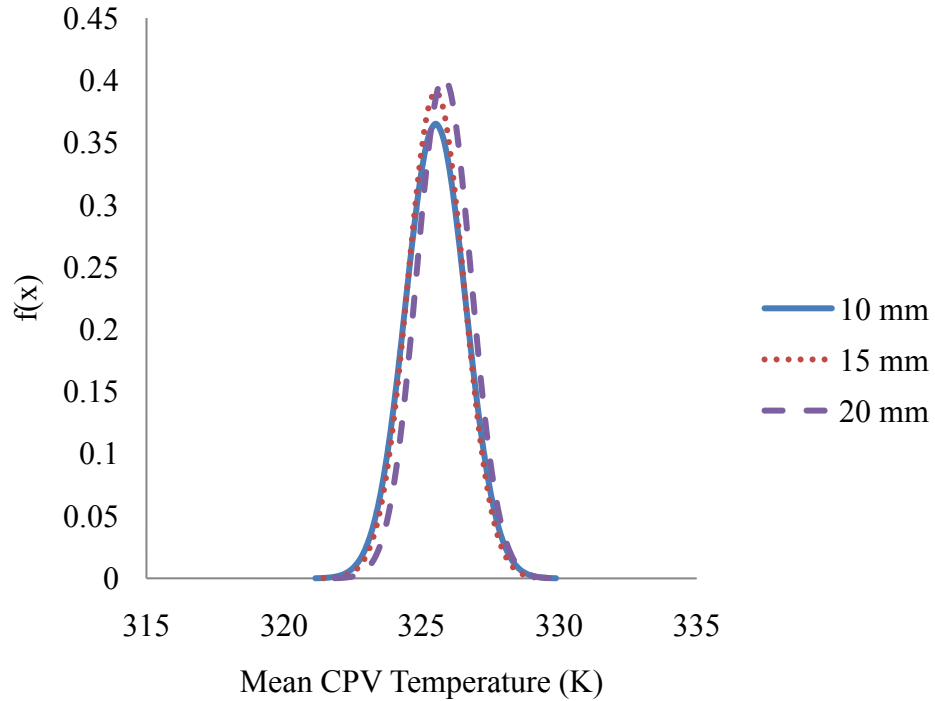


Figure 4.18: Effect of fin height on CPV temperature uniformity

4.9 Effect of Tip Clearance (Case Study 8)

The effect of tip clearance on maximum CPV temperature at different flow rate is depicted in Figure 4.19. Comparing the results of 1 and 3 mm height of tip clearance at the flow rate was $4 \times 10^{-4} \text{ m}^3/\text{s}$, a maximum temperature difference of only 0.14 K could be observed. Moreover, the effect declined gradually as the flow rate increased. For instance, at the flow rate of $12 \times 10^{-4} \text{ m}^3/\text{s}$, a temperature difference of only 0.07 K could be noticed. In conclusion, the numerical result indicated that the tip clearance had the minimum influence on the cooling performance compared to other parameters studied earlier in this work.

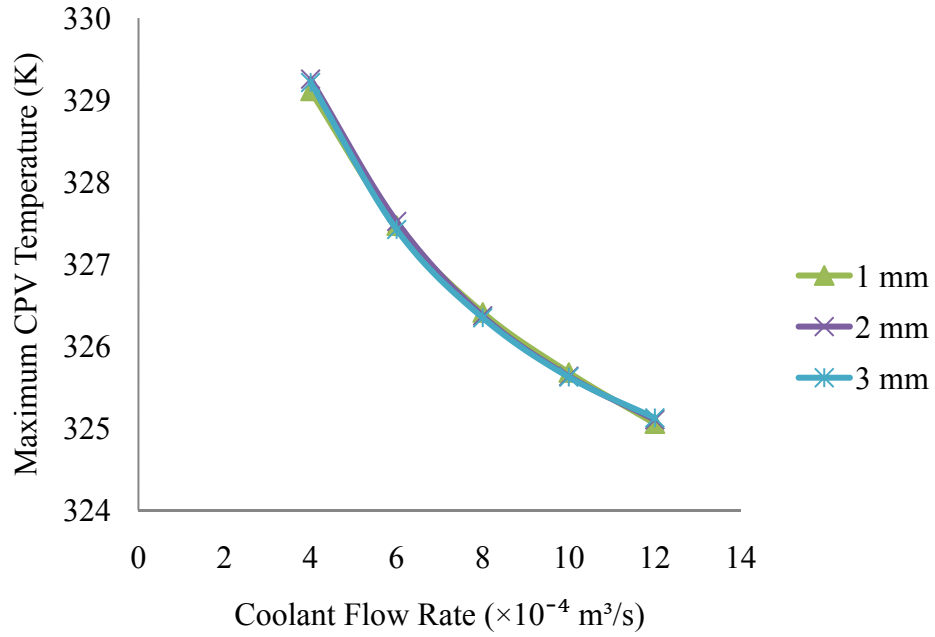


Figure 4.19: Effect of tip clearance on maximum CPV temperature

As shown in Figure 4.20, it could be learned that the effect of tip clearance on temperature uniformity was insignificant as well. By increasing the tip clearance from 1 to 3 mm, a slight improvement of 0.05 K on standard deviation could be observed.

Min et al. (2004) and Reyes et al. (2011) studied the effect of tip clearance on the cooling performance of plate fin heat sink. Both of them concluded that there was an optimum tip clearance which could lead to a better cooling performance. Min et al. (2004) found that the cooling performance was maximum (3.6 % improvement compared with heat sink without tip clearance) when tip clearance-to-channel width ratio was 0.6. Where else Reyes et al. (2011) found that the optimum tip clearance-to-channel width ratio ranged from 0.5 to 1.0. However, tip clearance was found to be less effective in current study. It should be highlighted that Type-2

design used in Case Study 8 had a center jet impingement inlet. Where else in the study conducted by Min et al. (2004) and Reyes et al. (2011), the coolant entered the heat sink from side. Hence, the different in inlet flow direction might be the reason for this phenomenon.

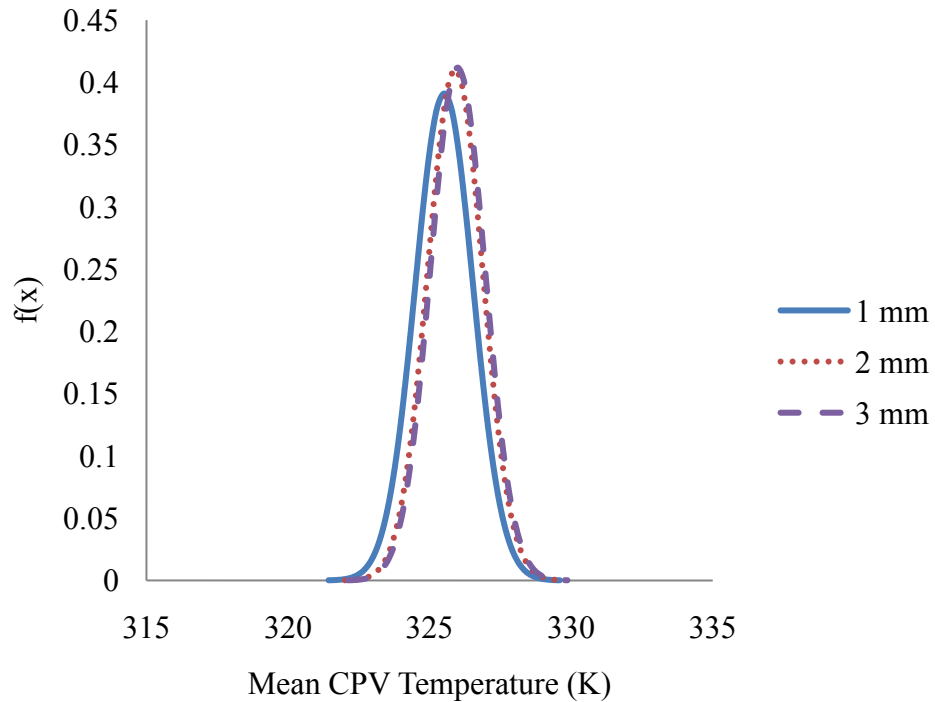


Figure 4.20: Effect of tip clearance on CPV temperature uniformity

Lastly, the results of the effects of flow and fin design parameters on cooling performance for each case study are summarized in Table 4.2. It should be noted that Type-1 cooling block with no fin split, which was identical with the cooling block installed at the site, was chosen to be as a base case in the comparisons of Case Studies 1 and 3.

Table 4.2: Summary of effects of different parameter on cooling performance

Case study	Change of parameters	Maximum CPV temperature	Temperature uniformity
1. Inlet/outlet arrangement			
• Type-1		Base case	Base case
• Type-2		Higher	Lower
• Type-3		Higher	Lower
• Type-4		Higher	Lower
• Type-5		Higher	Lower
2. Inlet flow rate	Increase	Decrease	Increase
3. Fin split			
• Type-1	No-split	Base case	Base case
	1-split	Higher	Lower
	2-split	Higher	Lower
	3-split	Higher	Lower
• Type-2	No-split	Higher	Lower
	1-split	Higher	Higher
	2-split	Higher	Higher
	3-split	Higher	Higher
• Type-3	No-split	Higher	Lower
	1-split	Higher	Higher
	2-split	Higher	Lower
	3-split	Higher	Higher
4. Fin width	Increase	Decrease	Increase
5. Fin spacing	Increase	Increase	Decrease
6. Inlet/outlet ratio	Increase	Increase	Decrease
7. Fin height	Increase	Less effective	Less effective
8. Tip clearance	Increase	Less effective	Less effective

CHAPTER 5

CONCLUSIONS AND FUTURE WORKS

5.1 Conclusions

This work was carried out with the objective of investigating the effects of different flow parameters and fin designs on the maximum operating temperature and temperature uniformity of the photovoltaic cells in a CPV system using three dimensional CFD simulation. On-site experimental data collected from a non-imaging planar concentrator was used to validate the result obtained from CFD simulations. Both results showed a good agreement.

In the study of effect of inlet/outlet arrangement, it could be noticed that it had a significant influence on the flow distribution of coolant in the cooling block. If the flow was able to distribute evenly and hence to maintain a higher flow velocity in each channel, the cooling performance could be improved. On the other hand, inlet flow rate also had a great influence on cooling performance. A higher flow rate has led to a lower thermal resistance between the coolant and cooling block. As a result, the system had a lower maximum operating temperature as well as a better temperature uniformity across the solar cells.

The introduction of fin split has been demonstrated to be able to enhance the performance of the cooling block with center jet impingement design as it allowed a more even distribution of flow. Besides, increment in the fin width as well as reduction of fin spacing improved the cooling performance as these were able to increase the total convective heat transfer area to encourage the heat to be effectively transferred from the cooling block to the coolant. As a result, it cooled the CPV cells. Lastly, it could be found that the fin height and tip clearance had insignificant effect on the cooling performance.

5.2 Contributions

This study presented the procedures and techniques for simulation of the 3D cooling block model for CPV system using CFD. The results, which were investigated for the first time, had clearly reflected the importance of each flow parameter and fin design on the maximum temperature and temperature uniformity for a dense array CPV. Hence, it is believed that the results of this study may help in designing an effective cooling block for a CPV system and resulting in better solar-to-electrical conversion efficiency, as well as preventing the system from permanent physical damage. The results could also be used as design guidelines with the benefit of saving the time for designing cooling system in the future.

Besides, the study also contributed to investigating the influence of inlet/outlet arrangement (Case Study 1), which had been conducted neither for the cooling of CPV, nor for a more general heat sink design. The works performed by other authors only focused on one flow direction. However, it was found in this study that inlet/outlet arrangement had exhibited great impact on cooling performance.

In addition, this study showed the first attempt to investigate the influence of inlet/outlet area ratio (Case Study 6) on the cooling of CPV. The results demonstrated a great improvement in the cooling performance. It should be therefore highlighted that the inlet/outlet area ratio should be taken into consideration when designing a cooling system for CPV in the future.

This study also contributed to the performance investigation of water-cooled system for CPV. Due to the high solar irradiance on the CPV cells, large amount of excessive thermal energy was stored in the cells. This had resulted in high increment in CPV temperature and it was found that an air-cooled system was no longer sufficient to remove the heat. Hence, liquid coolant that had a higher thermal conductivity than air was considered in this study. However, liquid-cooled system had a different fluid transfer mechanism compared to air-cooled system and should be enclosed to prevent electronics components from being damaged by the moisture.

5.3 Future Works

In current work, the study conducted was focused on the influences of various rectangular fin designs on the cooling block for a CPV system. Therefore, in order to design a novel and effective cooling system for a CPV, the following works can be conducted in the future.

Only a few previous studies have been conducted on the effect of fin shape on the cooling performance (Dogruoz et al., 2005; Yu et al., 2005; Khan et al., 2008; Huang and Chang, 2012; Yuan et al., 2012). The fin shapes including square pin fins, cylindrical pin fins, or a combination of different fin shapes can be considered in the future fin design in order to improve the distribution of coolant in the cooling block, and in turn enhance the cooling performance of a CPV system.

Denser fins can be placed in the high temperature zone of the cooling block in the future study to examine the flow patterns and heat transfer area, and eventually enhance the heat transfer and cool down the CPV located in the zone.

In addition, the base thickness of the cooling block should be designed to be thick enough to support the weight of CPV system and coolant, and thin enough to reduce thermal resistance. Therefore, an optimization analysis of the base thickness needs to be performed in the future study.

REFERENCES

Akbarzadeh, A. and Wadowski, T., 1996. Heat pipe-based cooling systems for photovoltaic cells under concentrated solar radiation. *Applied Thermal Engineering*, 16 (1), pp. 81-87.

Anderson, W. G., Dussinger, P. M., Sarraf, D. B. and Tamanna, S., 2008. Heat pipe cooling of concentrating photovoltaic cells. *Photovoltaic Specialists Conference*, 11-16 May 2008. pp. 1-6.

ANSYS 2011. ANSYS Fluent User's Guide. Canonsburg, PA: ANSYS, Inc.

Antón, I., Sala, G. and Pachón, D., Correction of the Voc vs. temperature dependence under non-uniform concentrated illumination. *17th European Photovoltaic Solar Energy Conference and Exhibition*, 2001. Munich, pp. 156-159.

Baig, H., Heasman, K. C. and Mallick, T. K., 2012. Non-uniform illumination in concentrating solar cells. *Renewable and Sustainable Energy Reviews*, 16 (8), pp. 5890-5909.

Ben Or, A. and Appelbaum, J., 2013. Performance analysis of concentrator photovoltaic dense-arrays under non-uniform irradiance. *Solar Energy Materials and Solar Cells*, 117 (0), pp. 110-119.

Bergman, T. L., Lavine, A. S., Incropera, F. P. and Dewitt, D. P., 2011. *Introduction to Heat Transfer*, 6th ed. U.S.: Wiley & Sons.

Brogren, M., 2004. *Optical efficiency of low-concentrating solar energy systems with parabolic reflectors*. PhD thesis, Uppsala University, Sweden.

Çengel, Y. A. and Cimbala, J. M., 2009. *Fluid Mechanics: Fundamentals and Applications*, 2nd ed. U.S.: McGraw-Hill Higher Education.

Chong, K.-K. and Tan, W.-C., 2012. Study of automotive radiator cooling system for dense-array concentration photovoltaic system. *Solar Energy*, 86 (9), pp. 2632-2643.

Chong, K. K., Siaw, F. L., Wong, C. W. and Wong, G. S., 2009. Design and construction of non-imaging planar concentrator for concentrator photovoltaic system. *Renewable Energy*, 34 (5), pp. 1364-1370.

Chow, T. T., 2010. A review on photovoltaic/thermal hybrid solar technology. *Applied Energy*, 87 (2), pp. 365-379.

Dalal, V. L. and Moore, A. R., 1977. Design considerations for high-intensity solar cells. *Journal of Applied Physics*, 48 (3), pp. 1244-1251.

Devore, J. L., 2000. *Probability and Statistics for Engineering and the Sciences*, 5th ed. USA: Duxbury.

Dogruoz, M. B., Urdaneta, M. and Ortega, A., 2005. Experiments and modeling of the hydraulic resistance and heat transfer of in-line square pin fin heat sinks with top by-pass flow. *International Journal of Heat and Mass Transfer*, 48 (23–24), pp. 5058-5071.

Gray, A., Boehm, R. and Stone, K. W., 2007. Modeling a Passive Cooling System for Photovoltaic Cells Under Concentration. *ASME/JSME 2007 Thermal Engineering Heat Transfer Summer Conference*, July 8–12 2007 Vancouver, British Columbia, Canada. pp. 447-454.

Holman, J. P., 2002. *Heat Transfer*, 9th ed. U.S.: McGraw-Hill.

Huang, C.-H. and Chang, W.-L., 2012. An inverse design method for optimizing design parameters of heat sink modules with encapsulated chip. *Applied Thermal Engineering*, 40 (0), pp. 216-226.

Khan, W. A., Culham, J. R. and Yovanovich, M. M., 2008. Modeling of Cylindrical Pin-Fin Heat Sinks for Electronic Packaging. *Components and Packaging Technologies, IEEE Transactions on*, 31 (3), pp. 536-545.

Li, H.-Y., Chao, S.-M. and Tsai, G.-L., 2005. Thermal performance measurement of heat sinks with confined impinging jet by infrared thermography. *International Journal of Heat and Mass Transfer*, 48 (25–26), pp. 5386-5394.

Li, H.-Y. and Chen, K.-Y., 2007. Thermal performance of plate-fin heat sinks under confined impinging jet conditions. *International Journal of Heat and Mass Transfer*, 50 (9–10), pp. 1963-1970.

Li, H.-Y., Chen, K.-Y. and Chiang, M.-H., 2009. Thermal-fluid characteristics of plate-fin heat sinks cooled by impingement jet. *Energy Conversion and Management*, 50 (11), pp. 2738-2746.

Luque, A., Sala, G. and Arboiro, J. C., 1998. Electric and thermal model for non-uniformly illuminated concentration cells. *Solar Energy Materials and Solar Cells*, 51 (3–4), pp. 269-290.

Luque, A. L., Andreev, V. M. and Viacheslav, A., 2007. *Concentrator Photovoltaics*. Springer.

Mathur, R. K., Mehrotra, D. R., Mittal, S. and Dhariwal, S. R., 1984. Thermal non-uniformities in concentrator solar cells. *Solar Cells*, 11 (2), pp. 175-188.

Mbewe, D. J., Card, H. C. and Card, D. C., 1985. A model of silicon solar cells for concentrator photovoltaic and photovoltaic/thermal system design. *Solar Energy*, 35 (3), pp. 247-258.

Min, J. Y., Jang, S. P. and Kim, S. J., 2004. Effect of tip clearance on the cooling performance of a microchannel heat sink. *International Journal of Heat and Mass Transfer*, 47 (5), pp. 1099-1103.

Natarajan, S. K., Mallick, T. K., Katz, M. and Weingaertner, S., 2011. Numerical investigations of solar cell temperature for photovoltaic concentrator system with and without passive cooling arrangements. *International Journal of Thermal Sciences*, 50 (12), pp. 2514-2521.

Reyes, M., Arias, J. R., Velazquez, A. and Vega, J. M., 2011. Experimental study of heat transfer and pressure drop in micro-channel based heat sinks with tip clearance. *Applied Thermal Engineering*, 31 (5), pp. 887-893.

Royne, A., Dey, C. J. and Mills, D. R., 2005. Cooling of photovoltaic cells under concentrated illumination: a critical review. *Solar Energy Materials and Solar Cells*, 86 (4), pp. 451-483.

Sala, G., 1989. Cooling of solar cells. Chapt. 8. In: E.R. PIKE, W. T. W. (ed.) *Solar cells and optics for photovoltaic concentration*. pp. 239-267.

Siaw, F.-L., Chong, K.-K. and Wong, C.-W., 2014. A comprehensive study of dense-array concentrator photovoltaic system using non-imaging planar concentrator. *Renewable Energy*, 62 (0), pp. 542-555.

Siddiqui, U. M., Arif, A. F. M., Kelley, L. and Dubowsky, S., 2012. Three-dimensional thermal modeling of a photovoltaic module under varying conditions. *Solar Energy*, 86 (9), pp. 2620-2631.

Skoplaki, E. and Palyvos, J. A., 2009. On the temperature dependence of photovoltaic module electrical performance: A review of efficiency/power correlations. *Solar Energy*, 83 (5), pp. 614-624.

Swanson, R. M., 2000. The promise of concentrators. *Progress in Photovoltaics: Research and Applications*, 8 (1), pp. 93-111.

Teo, H. G., Lee, P. S. and Hawlader, M. N. A., 2012. An active cooling system for photovoltaic modules. *Applied Energy*, 90 (1), pp. 309-315.

Wang, Y. N., Lin, T. T., Leong, J. C., Hsu, Y. T., Yeh, C. P., Lee, P. H. and Tsai, C. H., 2013. Numerical investigation of high-concentration photovoltaic module heat dissipation. *Renewable Energy*, 50 (0), pp. 20-26.

Xie, X. L., Liu, Z. J., He, Y. L. and Tao, W. Q., 2009. Numerical study of laminar heat transfer and pressure drop characteristics in a water-cooled minichannel heat sink. *Applied Thermal Engineering*, 29 (1), pp. 64-74.

Xing, W., Zhou, J. and Feng, Z., 2014. Effects of mounting geometries on photovoltaic module performance using CFD and single-diode model. *Solar Energy*, 103 (0), pp. 541-549.

Yu, X., Feng, J., Feng, Q. and Wang, Q., 2005. Development of a plate-pin fin heat sink and its performance comparisons with a plate fin heat sink. *Applied Thermal Engineering*, 25 (2-3), pp. 173-182.

Yuan, W., Zhao, J., Tso, C. P., Wu, T., Liu, W. and Ming, T., 2012. Numerical simulation of the thermal hydraulic performance of a plate pin fin heat sink. *Applied Thermal Engineering*, 48 (0), pp. 81-88.

Zhong, X., Fan, Y., Liu, J., Zhang, Y., Wang, T. and Cheng, Z., 2007. A Study of CFD Simulation for On-chip Cooling with 2D CNT Micro-fin Array. *High Density packaging and Microsystem Integration, International Symposium on*, 26-28 June 2007 Shanghai, China. IEEE, pp. 1-6.

Zhong, X., Wang, T., Liu, J., Zhang, Y. and Cheng, Z., 2006. Computational Fluid Dynamics Simulation for On-chip Cooling with Carbon Nanotube Micro-fin Architectures. *International Conference on Electronic Materials and Packaging*, 11-14 December 2006 Kowloon, China. IEEE, pp. 1-6.

Zhu, L., Wang, Y., Fang, Z., Sun, Y. and Huang, Q., 2010. An effective heat dissipation method for densely packed solar cells under high concentrations. *Solar Energy Materials and Solar Cells*, 94 (2), pp. 133-140.

APPENDIX

2012 International Conference on Innovation, Management and Technology Research (ICIMTR2012), Malacca, Malaysia :
21-22 May, 2012

A Study on Cooling of Concentrator Photovoltaic Cells using CFD

S. S. Lee
Department of Mechanical & Materials Engineering
Universiti Tunku Abdul Rahman
Kuala Lumpur, Malaysia
Email: lsshin@utar.edu.my

S. O. Lai
Department of Chemical Engineering
Universiti Tunku Abdul Rahman
Kuala Lumpur, Malaysia
Email: laiso@utar.edu.my

K. K. Chong
Department of Electrical & Electronic Engineering
Universiti Tunku Abdul Rahman
Kuala Lumpur, Malaysia
Email: chongkk@utar.edu.my

Abstract—Cooling of concentrator photovoltaic cells under high concentration of solar irradiance is one of the major challenges in designing concentrating photovoltaic system (CPV). Apart from the reduction of solar-to-electrical conversion efficiency, the highly excessive thermal energy generated may degrade the CPV and result in permanent damages. In this project, computational fluid dynamics (CFD) simulation has been performed to investigate the effects of different design parameters including inlet velocity, working fluid properties and cooling block geometry on thermal performance of the cooling system.

Keywords — Cooling; Computational Fluid Dynamics; Concentrator Photovoltaic Cells

I. INTRODUCTION

Construction cost for conventional photovoltaic cell system is high as the entire surface of the system is covered with expensive solar cells. Hence, concentrator photovoltaic cell (CPV) system has been introduced to reduce the cost by replacing the expensive photovoltaic cells with optical elements such as mirrors, which are in general less costly. However, during the operation of the CPV system, large amount of thermal energy will be generated. This thermal energy will in turn reduce the solar-to-electrical conversion efficiency, and even damage the solar cells if the temperature exceeds the allowable limit. Akbarzadeh and Wadowski [1] studied heat pipe based cooling systems for photovoltaic cells under concentrated solar radiation. They found that the solar cell performance decreased by 50% when the cell's surface temperature increased from 46°C to 84°C. Hence, an effective cooling system is very important to maximize the photovoltaic cells' efficiency and to prevent the cells from degradation and damage.

Computational fluid dynamics (CFD) simulation has been widely used to determine the thermal performance of a cooling system for CPV, computer heat sink and others. Gray and Stone [2] studied a passive cooling system for photovoltaic cells under concentration using CFD. They compared both simulation and experimental results and

found that the average difference is 3%. Anderson et al. [3] studied the cooling of concentrating photovoltaic systems, where heat pipes were used to deliver the waste heat to heat sinks attached and reject the heat through the fins by natural convection. A cooling system for a concentrated photovoltaic system has been developed by Mahderekal et al. [4], and their experimental and simulation results showed a good agreement. Yang et al. [5] built a photovoltaic wall test rig, which consisted of a massive wall, PV modules in front of the wall, an air duct between the PV modules and the wall, an air inlet and air outlet of the air duct, to validate the experimental results with the simulation results. The result showed that simulation model could be used to predict the thermal behaviour of PV wall and PV roof structures. Mohan and Govindarajan [6] have successfully applied CFD on investigating the thermal and flow analysis of different heat sinks mounted on CPU. Hence, it can be concluded that CFD is suitable to be used as a tool to study the performance of a CPV cooling system.

In this paper, CFD simulations were conducted to investigate the effects of different fin designs and flow parameters on the performance of CPV cooling system.

II. CFD MODELING

A three-dimensional simulation model, as shown in Figs 1(a) and (b) was developed using commercial software, Gambit. The computational domain consisted of three major parts, including cooling block, CPV with bonding layers and working fluid. The dimension of the copper cooling block was 350 mm (L) × 175 mm (W) × 20 mm (H), with identical square pin fins of width 5 mm and height 15 mm. Spacing between fins was 10.38 mm. The area of CPV was 280 mm (L) × 140 mm (W), with a height of 1.7 mm, including the bonding layers. Symmetric geometry of the copper cooling block (Fig. 2) was adopted to save the computational duration. A three-dimensional model having the same design but with larger spacing between fins, where fins were 15.19 mm apart, was used for simulation as well. Cooling block and working fluid were meshed using tetrahedral meshes,

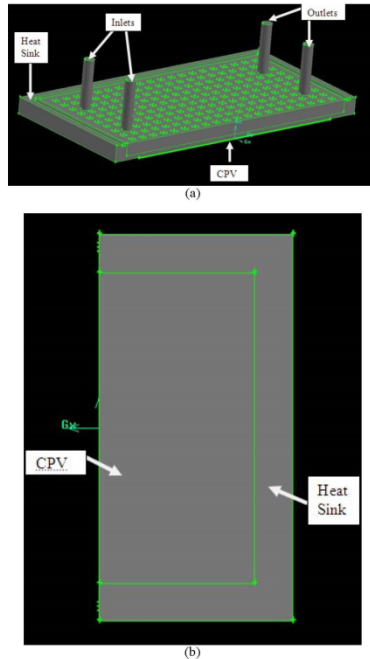


Figure 1. 3D model for simulation: (a) isometric view and (b) back view

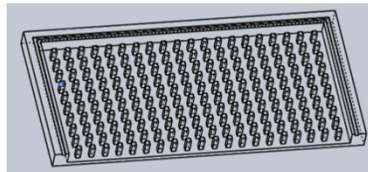


Figure 2. Symmetric geometry of square fin heat sink

while the CPV layers were meshed using hexagonal meshes.

In this symmetric model, the working fluid flew into the heat sink through two inlets and passed through the square fins to absorb the heat transferred from the CPV, and hence reduced the CPV temperature. Uniform heat flux of $255,000 \text{ W/m}^2$ was applied to the outer surface of CPV. The inlet velocity of working fluid ranged from 1.5 to 3.5 m/s and the inlet temperature was set to 300K.

Three dimensional CFD code (Fluent 6.3) was used to analyze the flow and temperature fields of the cooling block. Fluent solves the equations of mass, momentum and energy conservation using finite volume method.

$k-\epsilon$ turbulence model was used to represent the fluid flow.

The following assumptions were made: the system was in steady state, the flow was incompressible and turbulent, fluid and solid properties were constant and uniform heat flux on the bottom of the CPV, while all other external walls were perfectly insulated with no thermal radiation and convective heat transfer to the surrounding environment.

III. RESULTS AND DISCUSSION

In Fig. 3, it is worth noting that the maximum temperature did not appear at the center of the CPV, but was found towards the left. This was principally because the cooler working fluid entered the heat sink from the right hand side of the cooling block and it was able to absorb larger amount of heat as the temperature difference between the working fluid and the CPV was initially higher. As the working fluid flew through the cooling block, it absorbed more heat, resulting in lower temperature difference and high temperature at the left hand side region.

As shown in Figs. 4 (a) and (b), higher inlet velocity led to greater reduction in both average CPV and cooling block temperatures. The reductions of 8.36% and 10.55% on average CPV and cooling block temperatures, respectively, were noticed, when the inlet velocity was increased from 1.5 to 3.5 m/s. On the other hand, the cooling block with smaller spacing between fins performed better in terms of cooling performance, especially when the inlet velocity was low; nonetheless due to larger surface area for heat absorption, the effect faded gradually when the inlet velocity was elevated. When the inlet velocity was 1.5 m/s, a reduction of 46.3% in spacing between the fins (decreasing from 15.19 to 10.38 mm) reduced both average CPV and cooling block temperatures by 2.6% and 2.9%, respectively. However, the temperature differences caused by this spacing between fins were reduced to 0.6% and 0.9%, respectively when the inlet velocity was 3.5 m/s.

Thermal conductivity of water (0.6 W/m.K) was used as a reference. In Figs. 5 (a) and (b), the working fluid with thermal conductivity of 1 W/m.K reduced the average CPV and cooling block temperatures by 4.6% and 4.5%, respectively, when the inlet velocity was 1.5 m/s. At the same velocity, however, the working fluid with thermal conductivity of 0.5 W/m.K increased both average CPV and cooling block temperatures by 1.9%.

Figs. 6 (a) and (b) show the effects of viscosity of the

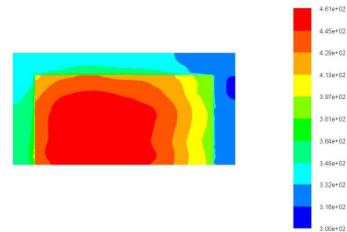


Figure 3. Contour of static temperature at inlet velocity of 1.5m/s

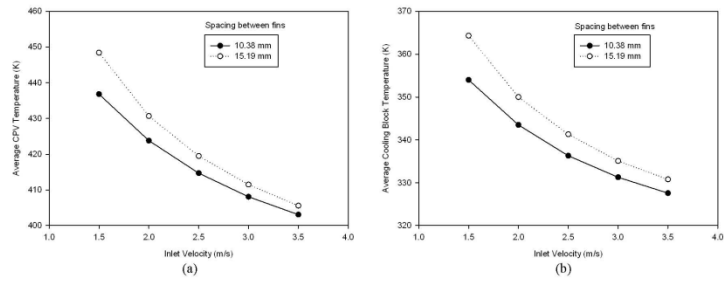


Figure 4. Effects of fin spacing and inlet velocity on (a) average CPV temperature and (b) average cooling block temperature

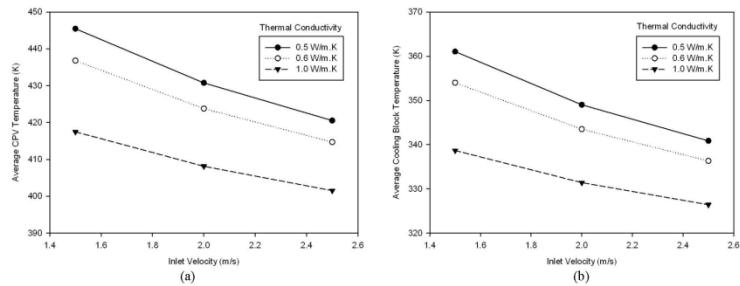


Figure 5. Effects of inlet velocity and working fluid thermal conductivity on (a) average CPV temperature and (b) average cooling block temperature

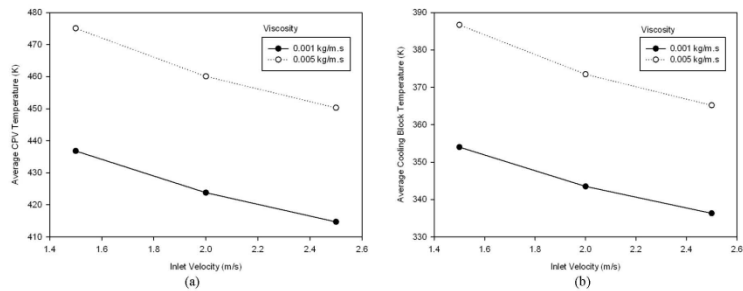


Figure 6. Effects of inlet velocity and working fluid viscosity on (a) average CPV temperature and (b) average cooling block temperature

working fluid on both average CPV and cooling block temperatures, respectively. It can be observed that the working fluid with lower viscosity had a better cooling performance.

IV. CONCLUSION

Computational fluid dynamics was successfully applied for the study of effects of different fin designs and flow

parameters on the performance of CPV cooling system. The results showed that low spacing between fins was important when the inlet velocity was low. Besides, high inlet velocity had a more significant effect on reducing the CPV temperature. The working fluid with high thermal conductivity and low viscosity would lead to better cooling performance.

ACKNOWLEDGMENT

The authors would like to acknowledge Universiti Tunku Abdul Rahman for their support.

REFERENCES

- [1] A. Akbarzadeh and T. Wadowski, "Heat pipe-based cooling systems for photovoltaic cells under concentrated solar radiation," *Applied Thermal Engineering*, vol. 16, no. 1, pp. 81-87, 1995.
- [2] A. Gray and K. W. Stone, "Modeling a passive cooling system for photovoltaic cells under concentration," in *2007 ASME-JSME Thermal Engineering Summer Heat Transfer Conference*, HT2007-32693.
- [3] W. G. Anderson, S. Tamanna, D. B. Sarraf, P. M. Dussinger and R. W. Hoffman, "Heat pipe cooling of concentrating photovoltaic (CPV) systems," in *8th International Energy Conversion Engineering Conference (IECEC)*, AIAA 2008-5672, 2008.
- [4] I. Mahderekal, C. K. Halford and R. F. Boehm, "Simulation and optimization of a concentrated photovoltaic system," *Journal of Solar Energy Engineering*, vol. 128, pp. 139-145, 2006.
- [5] H. X. Yang, R. H. Marshall and B. J. Brinkworth, "Validated simulation for thermal regulation of photovoltaic wall structures," in *Photovoltaic Specialists Conference, 1996, Conference Record of the Twenty Fifth IEEE*, pp. 1453-1456.
- [6] R. Mohan and Govindarajan, "Thermal and flow analysis of CPU with composite heat sinks using CFD," in *JCAAMB 2009*, Dec 14-16.
- [7] R. Anularasan and R. Velraj, "CFD analysis in a heat sink for cooling of electronic devices," *International Journal of The Computer, the Internet and Management*, vol. 16, no. 3, pp. 1-11, 2008.
- [8] M. A. Ismail, M. Z. Abdullah and M. A. Mijeebu, "A CFD-based experimental analysis on the effect of free stream cooling on the performance of micro processor heat sinks," *International Communications in Heat and Mass Transfer*, vol. 35, pp. 771-778, 2008.
- [9] R. L. Linton and D. Agonafer, "Coarse & detailed CFD modeling of a finned heat sink," *Components, Packaging, and Manufacturing Technology*, part A, vol. 18, issue 3, pp. 517-520, 1994.
- [10] A. Roync, C. J. Dey and D. R. Mills, "Cooling of photovoltaic cells under concentrated illumination: a critical review," *Solar Energy Materials & Solar Cells*, vol. 86, pp. 451-483, 2004.
- [11] L. Zhu, Y. Wang, Z. Fang, Y. Sun and Q. Huang, "An effective heat dissipation method for densely packed solar cells under high concentration," *Solar Energy Materials & Solar Cell*, vol. 94, pp. 133-140, 2010.